Fraunhofer Institut
Techno- und
Wirtschaftsmathematik

A. Wiegmann, A. Zemitis

EJ-HEAT:
A Fast Explicit Jump Harmonic Averaging Solver for the Effective Heat Conductivity of Composite Materials

Berichte des Fraunhofer ITWM, Nr. 94 (2006)

ISSN 1434-9973

Bericht 94 (2006)

Die Veröffentlichungen in der Berichtsreihe des Fraunhofer ITWM können bezogen werden über:

Fraunhofer-Institut für Techno- und
Wirtschaftsmathematik ITWM
Fraunhofer-Platz 1

67663 Kaiserslautern
Germany

Telefon: +49 (0) 6 31/3 16 00-0
Telefax: +49 (0) 6 31/3 16 00-10 99
E-Mail: info@itwm.fraunhofer.de
Internet: www.itwm.fraunhofer.de

Vorwort

Das Tätigkeitsfeld des Fraunhofer Instituts für Techno- und Wirtschaftsmathematik ITWM umfasst anwendungsnahe Grundlagenforschung, angewandte Forschung sowie Beratung und kundenspezifische Lösungen auf allen Gebieten, die für Techno- und Wirtschaftsmathematik bedeutsam sind.

In der Reihe »Berichte des Fraunhofer ITWM« soll die Arbeit des Instituts kontinuierlich einer interessierten Öffentlichkeit in Industrie, Wirtschaft und Wissenschaft vorgestellt werden. Durch die enge Verzahnung mit dem Fachbereich Mathematik der Universität Kaiserslautern sowie durch zahlreiche Kooperationen mit internationalen Institutionen und Hochschulen in den Bereichen Ausbildung und Forschung ist ein großes Potenzial für Forschungsberichte vorhanden. In die Berichtreihe sollen sowohl hervorragende Diplom- und Projektarbeiten und Dissertationen als auch Forschungsberichte der Institutsmitarbeiter und Institutsgäste zu aktuellen Fragen der Techno- und Wirtschaftsmathematik aufgenommen werden.

Darüberhinaus bietet die Reihe ein Forum für die Berichterstattung über die zahlreichen Kooperationsprojekte des Instituts mit Partnern aus Industrie und Wirtschaft.

Berichterstattung heißt hier Dokumentation darüber, wie aktuelle Ergebnisse aus mathematischer Forschungs- und Entwicklungsarbeit in industrielle Anwendungen und Softwareprodukte transferiert werden, und wie umgekehrt Probleme der Praxis neue interessante mathematische Fragestellungen generieren.

Prof. Dr. Dieter Prätzel-Wolters
Institutsleiter

Kaiserslautern, im Juni 2001

EJ-HEAT: A FAST EXPLICIT JUMP HARMONIC AVERAGING SOLVER FOR THE EFFECTIVE HEAT CONDUCTIVITY OF COMPOSITE MATERIALS

WE DEDICATE THIS WORK TO HELMUT NEUNZERT ON THE OCCASION OF HIS 70TH BIRTHDAY

A. WIEGMANN AND A. ZEMITIS
FRAUNHOFER ITWM
KAISERSLAUTERN

ABSTRACT. The stationary heat equation is solved with periodic boundary conditions in geometrically complex composite materials with high contrast in the thermal conductivities of the individual phases. This is achieved by harmonic averaging and explicitly introducing the jumps across the material interfaces as additional variables. The continuity of the heat flux yields the needed extra equations for these variables. A Schur-complent formulation for the new variables is derived that is solved using the FFT and BiCGStab methods.

The EJ-HEAT solver is given as a 3-page Matlab program in the Appendix. The C++ implementation is used for material design studies. It solves 3-dimensional problems with around 190 Mio variables on a 64-bit AMD Opteron desktop system in less than 6 GB memory and in minutes to hours, depending on the contrast and required accuracy.

The approach may also be used to compute effective electric conductivities because they are governed by the stationary heat equation.

Keywords: Stationary heat equation, effective thermal conductivity, explicit jump, discontinuous coefficients, virtual material design, microstructure simulation, EJ-HEAT

Date: September 6, 2006.

1991 *Mathematics Subject Classification.* 35J25,65N06,7327.

e-mail: wiegmann@itwm.fraunhofer.de, zemitis@itwm.fraunhofer.de

The authors are grateful for partial support by the Kaiserslautern Excellence Cluster Dependable Adaptive Systems and Mathematical Modeling.

1. Introduction

The goal of this work is to find a highly efficient and automated method to compute effective thermal conductivities for composite materials based on large 3d images on state of the art desktop computers without the need for any further processing, specifically without the need of additional mesh generation. In addition to the effective material property computation considered here, the methodology is also of interest whenever the solution of the steady or unsteady diffusion equation is needed, such as diffusion processes [7, 13, 17] or flows through porous media [3]

Modern imaging devices are capable of producing large three-dimensional data sets representing materials with resolution down to about 1 micron. Naturally, an interest arises in computing properties based on the microstructure [20, 15]. One possibility is to segment the volume image, or rectangular parallelepiped, into regions with constant grey values. The image points are interpreted to represent solid cubic cells (called *voxels*) with constant properties determined by the grey value. The segmented image already defines the computational mesh. Compared to the 2048^3-sized images from imaging devices we consider about one order of magnitude fewer variables. We give examples regarding the dependence of the effective thermal conductivity of composite materials on the distribution of the individual materials and on the contrast of conductivities between the different phases.

Since real materials are not usually periodic as assumed in the simulations, the choice of periodic boundary conditions introduces a deviation from measurable material properties. Other differences may result from other physical effects, such as convective or radiative heat transfer, or lack of resolution, to name a few possible sources.

The material as it enters the simulation is described by a rectangular parallelepiped of voxels. The physical resolution of the domain corresponds to the voxel length h. The same length h is also the resolution parameter of discretization. The numerics are performed on an equidistant Cartesian grid with temperature variables at the voxel centers. On each voxel the thermal conductivity is constant. For our method to work, we assume that the individual materials are isotropic, i.e. they conduct equally well in all directions. If two neighboring voxels correspond to different materials then the coefficient in the heat equation has a jump across the interface, namely the shared voxel face. Important features of this approach are

- the properties of each voxel are known,
- the positions of interfaces between two materials are easily determined voxel faces.

Figure 8 shows cross sections of 3d simulated closed pore foams. It illustrates that with sufficient resolution and enough voxels this discretization gives a reasonable model of the material. The images may stem from imaging devices or may be artificially generated. The approach may also be used to compute effective electric conductivities because they are also governed by the diffusion equation.

After a review on how to find the effective thermal conductivity, there three main points to the paper. The proposed method to solve the heat equation with discontinuous coefficients gives the same answer as the well-known harmonic averaging [16]. It is memory efficient enough to consider representative 3d portions of real media. It is fast enough to find the effective thermal conductivity of real media in acceptable time.

2. Equations

Heat transfer in materials purely due to diffusion is described by the heat equation

$$\nabla \cdot (\beta \nabla U) = f \text{ in } \Omega, \tag{1}$$

where U is the temperature, $\beta(\vec{x})$ is the local conductivity at $\vec{x} = (x_1, x_2, x_3)$, $\Omega = (0, d_1)\times(0, d_2)\times(0, d_3)$ is the rectangular parallelepiped, f models heat sources or sinks and $\nabla\cdot$ is the divergence operator $\left(\frac{\partial}{\partial x_1}, \frac{\partial}{\partial x_2}, \frac{\partial}{\partial x_3}\right)$.

To completely determine U, some boundary conditions are needed on the domain boundary $\partial\Omega$

2.1. Computing the effective thermal conductivity.

Each component material is assumed to be isotropic, that is conducting heat equally well in all spatial directions. Thus $\beta(\vec{x})$ is a scalar quantity. Due to geometric anisotropy, the effective thermal conductivity of the composite material is generally anisotropic and described by a tensor

$$\beta^* = \begin{bmatrix} \beta^*_{11} & \beta^*_{12} & \beta^*_{13} \\ \beta^*_{21} & \beta^*_{22} & \beta^*_{23} \\ \beta^*_{31} & \beta^*_{32} & \beta^*_{33} \end{bmatrix}.$$

This tensor can be determined by following homogenization theory for the estimation of β^*. In the 3D case [6], it is necessary to solve 3 different **singular periodic boundary value problems** ($l = 1, 2, 3$) in Ω:

$$\begin{aligned} \nabla \cdot (\beta(\vec{x})(\nabla U_l + \vec{e}_l)) = 0, \quad \vec{x} \in \Omega, \\ U_l(\vec{x} + id_1\vec{e}_1 + jd_2\vec{e}_2 + kd_3\vec{e}_3) = U_l(\vec{x}), \quad i, j, k \in \mathbf{Z} \end{aligned} \tag{2}$$

where $\vec{e}_l$ is a unit vector in the direction x_l. One finds three solutions U_1, U_2, U_3. The components of the averaged conductivity tensor can be found by integrating the inner product of the evaluation direction m against the flux and force in direction l:

$$\beta^*_{ml} = \frac{1}{d_1 d_2 d_3} \int_\Omega \langle \vec{e}_m, \beta(\vec{x})(\nabla U_l + \vec{e}_l) \rangle d\vec{x}, \quad l = 1, 2, 3; \quad m = 1, 2, 3, \tag{3}$$

where $\langle ., . \rangle$ denotes the inner product of two vectors. The main difficulty in this approach lies in solving the boundary value problem (2). As usual, the temperature is continuous. However, the heat flux $\beta \nabla U_l$ is continuous only in the directions perpendicular to $\vec{e}_l$ and has a jump in the direction $\vec{e}_l$ that is proportional to the difference in conductivities. This means the right hand side of (1), $f = -\nabla(\beta \vec{e}_l)$, is zero where β is constant, and singular along the discontinuities of β. This can be expressed as jump conditions

$$\begin{aligned} [U_l]|_{\vec{x}=\vec{x}^*} &= 0, \\ \left[\beta \frac{\partial U_l}{\partial x_i}\right]_{|_{\vec{x}=\vec{x}^*}} &= -\delta_{il} [\beta]_{\vec{x}=\vec{x}^*} \text{ for } i = 1, 2, 3, \end{aligned}$$

where ∂_{x_i} indicates the directional derivative in the ith coordinate direction, δ_{il} is the Kronecker symbol

$$\delta_{il} = \begin{cases} 1 & \text{for } i = l, \\ 0 & \text{for } i \neq l, \end{cases}$$

and $[g]_{\vec{x}=\vec{x}^*}$ is the jump in the term g across the interface at the position $\vec{x} = \vec{x}^*$.

2.2. **Analytic computation of the effective conductivity in the one-dimensional case.** In this case, the procedure of estimating the effective conductivity of a composite material simplifies to solving the auxiliary differential equation with periodic boundary conditions:

$$\frac{d}{dx}\left(\beta\left(\frac{dU}{dx} + 1\right)\right) = 0, \text{ for } x \in (0, 1), \tag{4}$$

$$U(0) = U(1), \tag{5}$$

$$\beta(0)\frac{\partial U}{\partial x}(0) = \beta(1)\frac{\partial U}{\partial x}(1) + (\beta(1) - \beta(0)); \tag{6}$$

and then computing the effective conductivity β^* by the weighted integration of the temperature derivative:

$$\beta^* = \int_0^1 \beta(x)\left(\frac{dU}{dx} + 1\right) dx. \tag{7}$$

We are interested in the case of piecewise constant $\beta(x)$. This means that the function $\beta(x)$ may have jumps, which occur on voxel faces. The second boundary condition is an interpretation of (4) that holds also if $\beta(0) \neq \beta(1)$ (a discontinuity may occur at the domain boundary) and ensures the continuity of $\frac{\partial U}{\partial x}$ if $\beta(0) = \beta(1)$. By using Dirac's Delta-function, equation (4) in the presence of m jumps at locations x_j can be re-written as

$$\frac{d}{dx}\left(\beta \frac{dU}{dx}\right) = -\sum_{j=1}^{m} [\beta]_j \delta(x - x_j), \quad x \in (0, 1).$$

The periodic boundary value problem (4)–(6) can be solved analytically. We consider a simple composite consisting of two materials with conductivities β_1 and β_2 where the number of jumps is $m = 2$, with notation $x_1 = a$ and $x_2 = b$.

$$\beta(x) = \begin{cases} \beta_1, & x \in [0, a], \\ \beta_2, & x \in (a, b), \\ \beta_1, & x \in [b, 1]. \end{cases}$$

The solution of (4)–(6) with this β is a piecewise linear function:

$$U(x) = \begin{cases} \lambda_0 + \lambda_1 x, & x \in [0, a], \\ \lambda_0 + \lambda_1 a + \lambda_2 (x - a), & x \in [a, b], \\ \lambda_0 + \lambda_1 (x - 1), & x \in [b, 1]. \end{cases}$$

This ansatz reflects the continuity of the temperature at a and continuity of the temperature and heat flux across the end-points already. The values λ_0, λ_1 and λ_2 can be found from the three additional conditions at the material interfaces: Continuity of the temperature at b, and discontinuity of fluxes at a and b. The first condition gives

$$\lambda_1 a + \lambda_2(b-a) = \lambda_1(b-1). \tag{8}$$

The two jump conditions for the flux both give the same equation:

$$\beta_2\lambda_2 - \beta_1\lambda_1 = \beta_1 - \beta_2. \tag{9}$$

In (8) and (9) only λ_1 and λ_2 are involved, they are found to be

$$\begin{aligned}\lambda_1 &= \frac{(b-a)(\beta_1-\beta_2)}{(b-a-1)\beta_2-(b-a)\beta_1},\\ \lambda_2 &= \frac{(b-a-1)(\beta_1-\beta_2)}{(b-a-1)\beta_2-(b-a)\beta_1}.\end{aligned}$$

The fact that λ_0 is undetermined exposes the typical behavior of the solutions to (4)–(6) not only in the one-dimensional case: due to periodic boundary conditions the solutions are only defined up to a constant. This fact is perfectly consistent with the computation of the effective properties via (7), because there only the gradient of the solution is involved.

To achieve uniqueness we are free to require that:

$$\int_0^1 U\, dx = 0.$$

This leads to the following determination of λ_0:

$$\lambda_0 = 0.5\lambda_1(b-1)^2 - 0.5\lambda_2(b-a)^2 - \lambda_1 a(b-a) - 0.5\lambda_1 a^2.$$

From this exact solution the effective conductivity coefficient is found from formula (7):

$$\beta^* = \beta_1(\lambda_1+1)(1+a-b) + \beta_2(b-a)(\lambda_2+1). \tag{10}$$

The generalization of this analytic solution to m jumps is straight-forward.

3. Discretization of the singular periodic boundary value problem (2)

The three domain lengths are co-measurable by construction, $d_1 = n_1 h$, $d_2 = n_2 h$ and $d_3 = n_3 h$. The grid points are the centers of the voxels, $\{0.5h, 1.5h, ..., (n_1-0.5)h\} \times \{0.5h, 1.5h, ..., (n_2-0.5)h\} \times \{0.5h, 1.5h, ..., (n_3-0.5)h\}$.

The variables have the following meaning: for $i = 1, 2, \ldots, n_1$, $j = 1, 2, \ldots, n_2$ and $k = 1, 2, \ldots, n_3$, lower case $u_{i,j,k}$ is the numerical solution value corresponding to upper case $U_{i,j,k} = U((i-\frac{1}{2})h, (j-\frac{1}{2})h, (k-\frac{1}{2})h)$.

Using the index map

$$I = i + n_1((j-1) + n_2(k-1)), \tag{11}$$

we identify u_I with $u_{i,j,k}$ for use in the linear algebra.

3.1. Notation for the jumps and their discretizations.

Again upper case $\left[\frac{\partial U}{\partial x_1}\right]_{i-\frac{1}{2},j,k}$ and $\left[\frac{\partial U}{\partial x_1}\right]_{i+\frac{1}{2},j,k}$ denote jumps in the x_1-derivative of U on the left and right walls of the (i,j,k) voxel, respectively. Similarly, $\left[\frac{\partial U}{\partial x_2}\right]_{i,j-\frac{1}{2},k}$, $\left[\frac{\partial U}{\partial x_2}\right]_{i,j+\frac{1}{2},k}$, $\left[\frac{\partial U}{\partial x_3}\right]_{i,j,k-\frac{1}{2}}$ and $\left[\frac{\partial U}{\partial x_3}\right]_{i,j,k+\frac{1}{2}}$ denote jumps in the x_2- and x_3-derivatives of U on the front and back walls and bottom and top walls of the (i,j,k) voxel, respectively.

Lower case $[\partial_{x_1}u]_{i-\frac{1}{2},j,k}$, $[\partial_{x_1}u]_{i+\frac{1}{2},j,k}$ $[\partial_{x_2}u]_{i,j-\frac{1}{2},k}$, $[\partial_{x_2}u]_{i,j+\frac{1}{2},k}$, $[\partial_{x_3}u]_{i,j,k-\frac{1}{2}}$ and $[\partial_{x_3}u]_{i,j,k+\frac{1}{2}}$ denote the discrete approximations of these quantitites.

3.2. Harmonic averaging.

The tensor product nature of the unidirectional centered differences on a Cartesian grid allows us to focus first on one space dimension. Consider

$$\frac{\partial}{\partial x}\left(\beta\frac{\partial}{\partial x}U\right) = f.$$

On a uniform Cartesian grid, this is discretized at the interior grid points $2 \le i \le n_1 - 1$ by harmonic averaging as follows:

$$\frac{1}{h}\left(\left(\frac{1}{2\beta_{i+1}}+\frac{1}{2\beta_i}\right)^{-1}\frac{u_{i+1}-u_i}{h} - \left(\frac{1}{2\beta_i}+\frac{1}{2\beta_{i-1}}\right)^{-1}\frac{u_i-u_{i-1}}{h}\right) = f_i. \tag{12}$$

The same formula may also be applied at the end points, for $i = 1$ and $i = n_1$, by identifying u_0 with u_{n_1} and u_{n_1+1} with u_1. For the three-dimensional case, similar differences in the other two directions are added to the discretization, see Lemma 2 below. This formulation stresses the fact that the harmonic averages of the conductivity at the location i with its left and right neighbors is computed [19, 16].

3.3. **Derivation via jump conditions.** Recall that $l \in \{1, 2, 3\}$ indicates the direction of the heat flux. We consider again

$$\nabla \cdot (\beta \nabla U) = -\nabla \cdot (\beta \vec{e_l}) .$$

By definition, the jump in the temperature gradient on voxel interfaces can be approximated with a first order accuracy in the following way:

$$\left[\frac{\partial U}{\partial x_1}\right]_{i+\frac{1}{2},j,k} = \frac{U_{i+1,j,k} - U_{i+\frac{1}{2},j,k}}{\frac{h}{2}} - \frac{U_{i+\frac{1}{2},j,k} - U_{i,j,k}}{\frac{h}{2}} + \mathcal{O}(h), \tag{13}$$

$$\left[\frac{\partial U}{\partial x_2}\right]_{i,j+\frac{1}{2},k} = \frac{U_{i,j+1,k} - U_{i,j+\frac{1}{2},k}}{\frac{h}{2}} - \frac{U_{i,j+\frac{1}{2},k} - U_{i,j,k}}{\frac{h}{2}} + \mathcal{O}(h), \tag{14}$$

$$\left[\frac{\partial U}{\partial x_3}\right]_{i,j,k+\frac{1}{2}} = \frac{U_{i,j,k+1} - U_{i,j,k+\frac{1}{2}}}{\frac{h}{2}} - \frac{U_{i,j,k+\frac{1}{2}} - U_{i,j,k}}{\frac{h}{2}} + \mathcal{O}(h). \tag{15}$$

Due to continuity the temperatures $U_{i+\frac{1}{2},j,k}$, $U_{i,j+\frac{1}{2},k}$ and $U_{i,j,k+\frac{1}{2}}$ at the interfaces are well defined. The jumps in the heat flux $\left[\beta\frac{\partial U}{\partial x_1}\right]_{i+\frac{1}{2},j,k}$, $\left[\beta\frac{\partial U}{\partial x_2}\right]_{i,j+\frac{1}{2},k}$ and $\left[\beta\frac{\partial U}{\partial x_3}\right]_{i,j,k+\frac{1}{2}}$ are discretized as

$$\beta_{i+1,j,k}\frac{U_{i+1,j,k} - U_{i+\frac{1}{2},j,k}}{\frac{h}{2}} - \beta_{i,j,k}\frac{U_{i+\frac{1}{2},j,k} - U_{i,j,k}}{\frac{h}{2}} = -\delta_{1l}(\beta_{i+1,j,k} - \beta_{i,j,k}) + \mathcal{O}(h), \tag{16}$$

$$\beta_{i,j+1,k}\frac{U_{i,j+1,k} - U_{i,j+\frac{1}{2},k}}{\frac{h}{2}} - \beta_{i,j,k}\frac{U_{i,j+\frac{1}{2},k} - U_{i,j,k}}{\frac{h}{2}} = -\delta_{2l}(\beta_{i,j+1,k} - \beta_{i,j,k}) + \mathcal{O}(h), \tag{17}$$

$$\beta_{i,j,k+1}\frac{U_{i,j,k+1} - U_{i,j,k+\frac{1}{2}}}{\frac{h}{2}} - \beta_{i,j,k}\frac{U_{i,j,k+\frac{1}{2}} - U_{i,j,k}}{\frac{h}{2}} = -\delta_{3l}(\beta_{i,j,k+1} - \beta_{i,j,k}) + \mathcal{O}(h). \tag{18}$$

As before, δ_{ml} is the Kronecker symbol. For ease of notation, we introduce

$$B_{i+\frac{1}{2},j,k} := \frac{\beta_{i+1,j,k} - \beta_{i,j,k}}{\beta_{i+1,j,k} + \beta_{i,j,k}}, \quad B_{i-\frac{1}{2},j,k} := \frac{\beta_{i,j,k} - \beta_{i-1,j,k}}{\beta_{i,j,k} + \beta_{i-1,j,k}}, \quad B_{1;i,j,k} := B_{i+\frac{1}{2},j,k} + B_{i-\frac{1}{2},j,k},$$

$$B_{i,j+\frac{1}{2},k} := \frac{\beta_{i,j+1,k} - \beta_{i,j,k}}{\beta_{i,j+1,k} + \beta_{i,j,k}}, \quad B_{i,j-\frac{1}{2},k} := \frac{\beta_{i,j,k} - \beta_{i,j-1,k}}{\beta_{i,j,k} + \beta_{i,j-1,k}}, \quad B_{2;i,j,k} := B_{i,j+\frac{1}{2},k} + B_{i,j-\frac{1}{2},k},$$

$$B_{i,j,k+\frac{1}{2}} := \frac{\beta_{i,j,k+1} - \beta_{i,j,k}}{\beta_{i,j,k+1} + \beta_{i,j,k}}, \quad B_{i,j,k-\frac{1}{2}} := \frac{\beta_{i,j,k} - \beta_{i,j,k-1}}{\beta_{i,j,k} + \beta_{i,j,k-1}}, \quad B_{3;i,j,k} := B_{i,j,k+\frac{1}{2}} + B_{i,j,k-\frac{1}{2}}.$$

Lemma 1. *A first order discretization of the condition of (dis-)continuity of the temperature gradient at the voxel interfaces is*

$$\left[\frac{\partial U}{\partial x_1}\right]_{i+\frac{1}{2},j,k} = -2\left(\frac{U_{i+1,j,k} - U_{i,j,k}}{h} + \delta_{1l}\right) B_{i+\frac{1}{2},j,k} + \mathcal{O}(h),$$

$$\left[\frac{\partial U}{\partial x_2}\right]_{i,j+\frac{1}{2},k} = -2\left(\frac{U_{i,j+1,k} - U_{i,j,k}}{h} + \delta_{2l}\right) B_{i,j+\frac{1}{2},k} + \mathcal{O}(h),$$

$$\left[\frac{\partial U}{\partial x_3}\right]_{i,j,k+\frac{1}{2}} = -2\left(\frac{U_{i,j,k+1} - U_{i,j,k}}{h} + \delta_{3l}\right) B_{i,j,k+\frac{1}{2}} + \mathcal{O}(h).$$

Proof. The formula follows from eliminating the auxiliary temperatures on the voxel faces from (16) - (18)

$$U_{i+\frac{1}{2},j,k} = \delta_{1l}\frac{h}{2}\frac{\beta_{i+1,j,k} - \beta_{i,j,k}}{\beta_{i+1,j,k} + \beta_{i,j,k}} + \frac{\beta_{i+1,j,k}U_{i+1,j,k}}{\beta_{i+1,j,k} + \beta_{i,j,k}} + \frac{\beta_{i,j,k}U_{i,j,k}}{\beta_{i+1,j,k} + \beta_{i,j,k}} + \mathcal{O}(h), \tag{19}$$

$$U_{i,j+\frac{1}{2},k} = \delta_{2l}\frac{h}{2}\frac{\beta_{i,j+1,k} - \beta_{i,j,k}}{\beta_{i+1,j,k} + \beta_{i,j,k}} + \frac{\beta_{i,j+1,k}U_{i,j+1,k}}{\beta_{i,j+1,k} + \beta_{i,j,k}} + \frac{\beta_{i,j,k}U_{i,j,k}}{\beta_{i,j+1,k} + \beta_{i,j,k}} + \mathcal{O}(h), \tag{20}$$

$$U_{i,j,k+\frac{1}{2}} = \delta_{3l}\frac{h}{2}\frac{\beta_{i+1,j,k} - \beta_{i,j,k}}{\beta_{i+1,j,k} + \beta_{i,j,k}} + \frac{\beta_{i,j,k+1}U_{i,j,k+1}}{\beta_{i,j,k+1} + \beta_{i,j,k}} + \frac{\beta_{i,j,k}U_{i,j,k}}{\beta_{i,j,k+1} + \beta_{i,j,k}} + \mathcal{O}(h). \tag{21}$$

These values are used in (13) - (15). □

Knowing the discontinuities in the temperature gradient, one can adjust the temperatures in the neighboring cells so that the corrected u is locally a discretization of a smooth function, as in the Immersed Interface [11, 23] and Ghost Fluid methods [4]. Then one would like to divide by the conductivity as in the case of constant β and to maintain only the jump conditions. Recall that for constant β,

$$\nabla \cdot (\beta \nabla U) = \beta \Delta U.$$

Using Taylor expansions in the presence of jumps (Lemma 3 in [23]), one finds

$$\begin{aligned}\frac{\beta_{i,j,k}}{h}\Bigg(&\frac{\left(U_{i+1,j,k}-\frac{h}{2}\left[\partial_{x_1}U\right]_{i+\frac12,j,k}\right)-u_{i,j,k}}{h}-\frac{U_{i,j,k}-\left(U_{i-1,j,k}-\frac{h}{2}\left[\partial_{x_1}U\right]_{i-\frac12,j,k}\right)}{h}\\ &+\frac{\left(U_{i,j+1,k}-\frac{h}{2}\left[\partial_{x_2}U\right]_{i,j+\frac12,k}\right)-U_{i,j,k}}{h}-\frac{U_{i,j,k}-\left(U_{i,j-1,k}-\frac{h}{2}\left[\partial_{x_2}U\right]_{i,j-\frac12,k}\right)}{h}\\ &+\frac{\left(U_{i,j,k+1}-\frac{h}{2}\left[\partial_{x_3}U\right]_{i,j,k+\frac12}\right)-U_{i,j,k}}{h}-\frac{U_{i,j,k}-\left(U_{i,j,k-1}-\frac{h}{2}\left[\partial_{x_3}U\right]_{i,j,k-\frac12}\right)}{h}\Bigg) \quad = \quad \mathcal{O}(h).\end{aligned} \tag{22}$$

Note that in (22) the right hand side is $\mathcal{O}(h)$, the singular contributions in direction l are absorbed into the definition of the jumps. As usual, for the discrete problem the order terms are simply dropped, and the solution of the continuous problem $U_{i,j,k}$ is replaced by the discrete variables $u_{i,j,k}$.

Lemma 2. *Equation (22) with zero right hand side is the harmonic averaging discretization (12) in 3 dimensions,*

$$\begin{aligned}\frac{1}{h}\Bigg(&\left(\frac{1}{2\beta_{i+1,j,k}}+\frac{1}{2\beta_{i,j,k}}\right)^{-1}\frac{u_{i+1,j,k}-u_{i,j,k}}{h}-\left(\frac{1}{2\beta_{i,j,k}}+\frac{1}{2\beta_{i-1,j,k}}\right)^{-1}\frac{u_{i,j,k}-u_{i-1,j,k}}{h}\\ &+\left(\frac{1}{2\beta_{i,j+1,k}}+\frac{1}{2\beta_{i,j,k}}\right)^{-1}\frac{u_{i,j+1,k}-u_{i,j,k}}{h}-\left(\frac{1}{2\beta_{i,j,k}}+\frac{1}{2\beta_{i,j-1,k}}\right)^{-1}\frac{u_{i,j,k}-u_{i,j-1,k}}{h}\\ &+\left(\frac{1}{2\beta_{i,j,k+1}}+\frac{1}{2\beta_{i,j,k}}\right)^{-1}\frac{u_{i,j,k+1}-u_{i,j,k}}{h}-\left(\frac{1}{2\beta_{i,j,k}}+\frac{1}{2\beta_{i,j,k-1}}\right)^{-1}\frac{u_{i,j,k}-u_{i,j,k-1}}{h}\Bigg) \quad = \quad f_{i,j,k}\end{aligned} \tag{23}$$

with right hand side

$$f_{i,j,k} = -\frac{\beta_{i,j,k}}{h}\left(\delta_{1l}B_{1;i,j,k}+\delta_{2l}B_{2;i,j,k}+\delta_{3l}B_{3;i,j,k}\right). \tag{24}$$

Proof. We show the portion of the identity only for the first term in (22), the others follow in the same way.

$$\begin{aligned}&\frac{\beta_{i,j,k}}{h}\left(\frac{\left(u_{i+1,j,k}-\frac{h}{2}\left[\partial_{x_1}u\right]_{i+\frac12,j,k}\right)-u_{i,j,k}}{h}\right)\\ =\;&\frac{\beta_{i,j,k}}{h^2}\left(\left(1+B_{i+\frac12,j,k}\right)u_{i+1,j,k}-\left(B_{i+\frac12,j,k}+1\right)u_{i,j,k}+h\delta_{1l}B_{i+\frac12,j,k}\right)\\ =\;&\frac{\beta_{i,j,k}}{h^2}\left(2\frac{\beta_{i+1,j,k}}{\beta_{i+1,j,k}+\beta_{i,j,k}}u_{i+1,j,k}-2\frac{\beta_{i+1,j,k}}{\beta_{i+1,j,k}+\beta_{i,j,k}}u_{i,j,k}+h\delta_{1l}B_{i+\frac12,j,k}\right)\\ =\;&\frac{1}{h}\left(\frac{1}{2\beta_{i+1,j,k}}+\frac{1}{2\beta_{i,j,k}}\right)^{-1}\frac{u_{i+1,j,k}-u_{i,j,k}}{h}+\frac{\beta_{i,j,k}}{h}\delta_{1l}B_{i+\frac12,j,k}.\end{aligned} \tag{25}$$

□

Note that (24) is valid for all i, j, k because $f_{i,j,k} = 0$ where β is constant. The contributions to $f_{i,j,k}$ come only from the direction l. No contributions are made in the other two directions where the multiplication with $\vec{e}_l$ wipes out any discontinuity in β. Note that $f_{i,j,k}$ is proportional to h^{-1}, indicating the δ-singularity of the force also in the discrete setting.

3.4. **Discretization of the 1d problem.** Compared with §2.2, the discretization allows only special locations for the discontinuity, namely on the voxel boundaries. This restriction is made strictly in order to devise an efficient and robust method, the general case of arbitrary locations was treated in [23], which contains the details on how to derive jump corrected differences based on Taylor expansions in the presence of discontinuities.

The general formula at the point x_i simplifies to

$$\frac{\beta_i}{h}\left(\frac{\left(u_{i+1}-\frac{h}{2}\left[u_x\right]_{i+\frac{1}{2}}\right)-u_i}{h}-\frac{u_i+\left(\frac{h}{2}\left[u_x\right]_{i-\frac{1}{2}}-u_{i-1}\right)}{h}\right)=f_i$$

and is then rewritten as

$$\frac{u_{i+1}-2u_i+u_{i-1}}{h^2}-\frac{\left[u_x\right]_{i+\frac{1}{2}}+\left[u_x\right]_{i-\frac{1}{2}}}{2h}=\frac{f_i}{\beta_i}.$$

In these formulas the factor $\frac{h}{2}$ in front of the jumps is the distance of the cell wall from the cell center. The discretization of the jump condition simplifies to

$$\left[u_x\right]_{x_{i+\frac{1}{2}}}+\frac{2(\beta^+-\beta^-)}{\beta^++\beta^-}\frac{u_{i+1}-u_i}{h}=-\frac{2(\beta^+-\beta^-)}{\beta^++\beta^-}.$$

4. Schur-complement

In harmonic averaging, (23) is solved, which in our context may be viewed as eliminating the jump variables from the extended system, and forming the Schur-complement for the original variables. Here we propose the opposite: eliminating the solution variables, and only keeping the jump variables.

4.1. **Derivation of the Schur-complement for the jumps.** Dividing (22) by $\beta_{i,j,k}$ and reorganizing (19) - (19), we summarize the discretization of (2) with explicit jumps as discretization of the partial differential equation and discretization of the jump conditions

$$\begin{aligned}
&\frac{u_{i+1,j,k}+u_{i-1,j,k}}{h^2}-\frac{\left[\partial_{x_1}u\right]_{i+\frac{1}{2},j,k}+\left[\partial_{x_1}u\right]_{i-\frac{1}{2},j,k}}{2h}+\\
&+\frac{u_{i,j+1,k}+u_{i,j-1,k}}{h^2}-\frac{\left[\partial_{x_2}u\right]_{i,j+\frac{1}{2},k}+\left[\partial_{x_2}u\right]_{i,j-\frac{1}{2},k}}{2h}+\\
&+\frac{u_{i,j,k+1}+u_{i,j,k-1}}{h^2}-\frac{\left[\partial_{x_3}u\right]_{i,j,k+\frac{1}{2}}+\left[\partial_{x_3}u\right]_{i,j,k-\frac{1}{2}}}{2h}-\frac{6u_{i,j,k}}{h^2} &= 0, \qquad (26)\\
&2B_{i+\frac{1}{2},j,k}\frac{u_{i+1,j,k}-u_{i,j,k}}{h}+\left[\partial_{x_1}u\right]_{i+\frac{1}{2},j,k} &= -2\delta_{1l}B_{i+\frac{1}{2},j,k}, \qquad (27)\\
&2B_{i-\frac{1}{2},j,k}\frac{u_{i,j,k}-u_{i-1,j,k}}{h}+\left[\partial_{x_1}u\right]_{i-\frac{1}{2},j,k} &= -2\delta_{1l}B_{i-\frac{1}{2},j,k}, \qquad (28)\\
&2B_{i,j+\frac{1}{2},k}\frac{u_{i,j+1,k}-u_{i,j,k}}{h}+\left[\partial_{x_2}u\right]_{i,j+\frac{1}{2},k} &= -2\delta_{2l}B_{i,j+\frac{1}{2},k}, \qquad (29)\\
&2B_{i,j-\frac{1}{2},k}\frac{u_{i,j,k}-u_{i,j-1,k}}{h}+\left[\partial_{x_2}u\right]_{i,j-\frac{1}{2},k} &= -2\delta_{2l}B_{i,j-\frac{1}{2},k}, \qquad (30)\\
&2B_{i,j,k+\frac{1}{2}}\frac{u_{i,j,k+1}-u_{i,j,k}}{h}+\left[\partial_{x_3}u\right]_{i,j,k+\frac{1}{2}} &= -2\delta_{3l}B_{i,j,k+\frac{1}{2}}, \qquad (31)\\
&2B_{i,j,k-\frac{1}{2}}\frac{u_{i,j,k}-u_{i,j,k-1}}{h}+\left[\partial_{x_3}u\right]_{i,j,k-\frac{1}{2}} &= -2\delta_{3l}B_{i,j,k-\frac{1}{2}}. \qquad (32)
\end{aligned}$$

As before, the Kronecker delta δ_{ml} indicates that a source term is active only when the homogenization equation (2) is driven in direction l.

Where the jumps are zero due to continuity of β, the equation (27), (28), ... or (32) is simply dropped from the system, and the jump term is dropped from (26). Even doing this, the structure of the system (26) can always be expressed as

$$\begin{bmatrix} A & \Psi \\ D & I \end{bmatrix}\begin{bmatrix} \mathbf{U} \\ J \end{bmatrix}=\begin{bmatrix} 0 \\ F_2 \end{bmatrix},$$

where $\mathbf{U}$ is the vector of temperatures at the grid points and J is the vector of nontrivial jumps where β is discontinuous. We define the length of J as $m=m_1+m_2+m_3$, where the m_i indicate the numbers of discontinuities in β in the three coordinate directions, respectively. The length of $\mathbf{U}$ is $n=n_1n_2n_3$. $A\in\mathbf{R}^{n\times n}$ is the matrix of the 7-point discretization of the Laplacian with periodic boundary conditions and *is not invertible*. $A\mathbf{U}=F$ is the discretization of the Poisson problem. $\Psi\in\mathbf{R}^{n\times m}$ embeds the jumps with coefficient $-\frac{1}{2h}$ in the rows corresponding to the two voxels that neighbor the discontinuity. $I\in\mathbf{R}^{m\times m}$ is the identity matrix and $D\in\mathbf{R}^{m\times n}$ applies the coefficients of the discretizations of the jump conditions to the temperature variables.

In principle, the ordering of the temperatue and jump variables could be arbitrary. But in order to use the FFT, they should be ordered according to (11). The order of the jump variables follows the same pattern,

but first collecting the jumps in the x_1, then the jumps in the x_2 and finally the jumps in the x_3 direction. The precise details can be found in the matlab program in Appendix A.

A is invertible on $\mathbf{R}^n/\{\mathbf{x}\in\mathbf{R}^n : \sum \mathbf{x}=0\}$. We denote the Pseudo inverse by $A^\dagger$ and recall from [22] that it can be applied efficiently using Fast Poisson solvers based on the FFT. We denote the Fourier transform of the solution by $\hat{\mathbf{U}}_{i,j,k}$. It can be obtained from the three-dimensional Fourier transform of the right hand side $\hat{F}_{i,j,k}$:

$$\hat{\mathbf{U}}_{i,j,k} = \frac{\hat{F}_{i,j,k}h^2}{2\cos\left(\frac{2\pi(i-1)}{n_1}\right)+2\cos\left(\frac{2\pi(j-1)}{n_2}\right)+2\cos\left(\frac{2\pi(k-1)}{n_3}\right)-6}.$$

This illustrates clearly the kernel and range of A. The denominator is zero if and only if $i=j=k=1$. This Fourier mode corresponds to the sum of F and $\mathbf{U}$, respectively. A solution exists if $\sum F=0$. In this case $\mathbf{U}$ with $\sum \mathbf{U}=0$ is the unique solution.

First, we observe that for any of the directions $l=1,2,3$ we always have $\sum F_2=0$. Also, $\sum D\mathbf{U}=0$ for all $\mathbf{U}\in\mathbf{R}^n$. This implies that if a solution $(\mathbf{U},J)$ exists, its second component J must satisfy $\sum J=0$. But $\sum J=0$ implies that $\sum \Psi J=0$, so that $-\Psi J$ is in the range of A.

So, the Pseudo Schur-complement for the jump variables

$$\left(I-DA^\dagger\Psi\right)J=F_2 \tag{33}$$

inherits the solution from that of the original harmonic averaging formulation.

4.2. **Efficient Schur-complement multiplication.** The system (33) is non-symmetric and solved iteratively by the BiCGStab variant of the conjugate gradient method [21] following [9]. This allows to avoid forming the Schur-complement matrix explicitly, but rather performs the needed matrix-vector multiplication as

$$\begin{aligned} y_1 &= \Psi J^{(n)},\\ y_2 &= A^\dagger y_1,\\ y_3 &= Dy_2,\\ y_4 &= J^{(n)}-y_3. \end{aligned}$$

From the solution J of (33) the temperatures are found as

$$\mathbf{U}=-A^\dagger\Psi J.$$

To evaluate the quality of the computed temperature field, one evaluates the relative residual error of the large Schur-complement, up to the factor β the harmonic averaging formulation (23).

$$(A-\Psi D)\,\mathbf{U}=-\Psi F_2,$$

i.e.

$$R_{rel}=\frac{\|\,(A-\Psi D)\,\mathbf{U}+\Psi F_2\|_2}{\|\Psi F_2\|_2}.$$

5. Evaluation of the effective thermal conductivity

After the 3 problems (2) for temperature and jumps in the heat flux from §2 are solved, the tensor of effective thermal conductivity can be obtained approximating the integral (3) as

$$\beta_{ml}\approx\frac{1}{d_1d_2d_3}\sum_{i=1}^{n_1}\sum_{j=1}^{n_2}\sum_{k=1}^{n_3}\beta_{i,j,k}(D_{m;i,j,k}+\delta_{ml})h^3,$$

where

$$\begin{aligned} D_{1;i,j,k} &= \frac{u_{i+1,j,k}-u_{i-1,j,k}}{2h}-\frac{[\partial_{x_1}u]_{i+\frac12,j,k}-[\partial_{x_1}u]_{i-\frac12,j,k}}{4},\\ D_{2;i,j,k} &= \frac{u_{i,j+1,k}-u_{i,j-1,k}}{2h}-\frac{[\partial_{x_2}u]_{i,j+\frac12,k}-[\partial_{x_2}u]_{i,j-\frac12,k}}{4},\\ D_{3;i,j,k} &= \frac{u_{i,j,k+1}-u_{i,j,k-1}}{2h}-\frac{[\partial_{x_3}u]_{i,j,k+\frac12}-[\partial_{x_3}u]_{i,j,k-\frac12}}{4}. \end{aligned}$$

In the case of continuous heat fluxes on the voxel faces the formulas reduce to the standard central differences for the first derivatives. The periodicity of the domain is taken into account by identifying subscripts 0 with n_1, n_2 or n_3, respectively, and subscripts n_1+1, n_2+1 or n_3+1 with 1.

5.1. **Numerical solution of the one-dimensional example.** We consider the periodic layered media from §2.2 and §3.4 for the special case $a = 1/3$ and $b = 1$ with coefficients $\beta_1 = 1$, $\beta_2 = 5$. As mesh width we choose $h = 1/3$. Thus we have only 3 unknown function values $\{u_i \mid i = 1, 2, 3\}$ at locations 1/6, 3/6 and 5/6 and 2 unknown jumps $\{J_i \mid i = 1, 2\}$ for derivatives on the interfaces. The material with conductivity β_1 consists only of a single cell, which must sustain two jumps on its two sides, with one jump location coinciding with the periodic domain boundary.

The discretized system for this example is the following:

$$\begin{bmatrix} -\frac{2}{h^2} & \frac{1}{h^2} & \frac{1}{h^2} & -\frac{1}{2h} & -\frac{1}{2h} \\ \frac{1}{h^2} & -\frac{2}{h^2} & \frac{1}{h^2} & 0 & -\frac{1}{2h} \\ \frac{1}{h^2} & \frac{1}{h^2} & -\frac{2}{h^2} & -\frac{1}{2h} & 0 \\ -2\frac{(\beta_1-\beta_2)}{(\beta_1+\beta_2)h} & 0 & 2\frac{(\beta_1-\beta_2)}{(\beta_1+\beta_2)h} & 1 & 0 \\ 2\frac{(\beta_2-\beta_1)}{(\beta_2+\beta_1)h} & -2\frac{(\beta_2-\beta_1)}{(\beta_2+\beta_1)h} & 0 & 0 & 1 \end{bmatrix} \begin{bmatrix} u_1 \\ u_2 \\ u_3 \\ J_1 \\ J_2 \end{bmatrix} = \begin{bmatrix} 0 \\ 0 \\ 0 \\ -2\frac{(\beta_1-\beta_2)}{(\beta_1+\beta_2)h} \\ -2\frac{(\beta_2-\beta_1)}{(\beta_2+\beta_1)h} \end{bmatrix}$$

The matrix of this linear system of equations is singular. More precisely, it inherits this feature from the upper left submatrix that corresponds to the Laplace operator with periodic boundary conditions. Note that the right hand side of the system lies in the range of the matrix. Thus, the solution exists and can be made unique by requiring that it must sum to zero. The solution is $u_1 = 0$, $u_2 = 2/21$, $u_3 = -2/21$, $J_1 = -12/7$ and $J_2 = 12/7$. Because in this simple case the solution is piecewise linear, the discrete system gives exact values of the solution. Also the effective conductivity coefficient can be estimated exactly from the discrete solution.

The effective conductivity can be estimated centrally by the formula:

$$\beta^* = \sum_{i=1}^{n} \left(\frac{u_{i+1} - u_{i-1}}{h} - \frac{1}{2} \left[\partial_x u\right]_{i+\frac{1}{2}} + \frac{1}{2} \left[\partial_x u\right]_{i-\frac{1}{2}} + 1 \right) \beta_i h.$$

where $[u_x]_{i+\frac{1}{2}} = 0$ if voxels with the centers a x_i and x_{i+1} correspond to the same material, $[u_x]_{i-\frac{1}{2}} = 0$ if voxels with the centers at x_i and x_{i-1} correspond to the same material, the u_{n+1} variable is identified with the u_1 variable and the u_0 variable is identified with the u_n variable.

For the given example $n = 3$ and the formula can be written explicitly:

$$\beta^* = \beta_1 h \left(\frac{u_2 - u_3}{h} - \frac{1}{2} J_2 + \frac{1}{2} J_1 + 1 \right) + \beta_2 h \left(\frac{u_3 - u_1}{h} + \frac{1}{2} J_2 + 1 \right) + \beta_2 h \left(\frac{u_1 - u_2}{h} - \frac{1}{2} J_1 + 1 \right).$$

In this example the effective coefficient is: $\beta^* = 15/7$, in agreement with (10).

6. Examples

6.1. **Example: Layered media.** Consider the infinite layered media in 2 dimensions with period length 5 and contrast c,

$$\beta(x, y) = \begin{cases} c: & y \in \bigcup_{k=-\infty}^{\infty} [5k, 2 + 5k) \\ 1: & y \in \bigcup_{k=-\infty}^{\infty} [2 + 5k, 5 + 5k) \end{cases}.$$

Figure **??** shows this media with three finite computational domains that are periodicity cells for this media, i.e. each of them tiles the plane. The angles and mesh widths are chosen so that in all cases for all refinements the volume fractions are preserved precisely, i.e. 40% gray and 60% white area. This eliminates the biggest source of possible error, as the volume fration is known to be the dominating influence on the effective conductivity [20].

The first domain, with coarsest grid voxel centers marked with '+' symbols in Figure **??**, is oriented in agreement with the orientation of the media. In this case, the numerical method results in the exact values for the effective conductivity

$$\beta^* = \begin{bmatrix} \beta^*_{\eta\eta} & 0 \\ 0 & \beta^*_{\xi\xi} \end{bmatrix}, \tag{34}$$

where $\beta^*_{\eta\eta} = \frac{2}{5} \cdot c + \frac{3}{5} \cdot 1$ is the arithmetic mean and $\beta^*_{\xi\xi} = \left(\frac{2}{5} \cdot \frac{1}{c} + \frac{3}{5} \cdot \frac{1}{1} \right)^{(-1)}$ is the harmonic mean of the conductivities.

Now let α denote the angle by which the media is rotated against the computational domain. In Figure **??**, the cases $\alpha = 0$, $\alpha = -\pi/4$ and $\alpha = -\arctan(2/5)$ are shown. The respective computational domains are illustrated by coarsest grid center voxels marked by '+', '$*$' and '$\times$' symbols, respectively. Figure 2 shows the domain for $\alpha = -\arctan(2/5)$ for the three coarsest resolutions that we consider in the numerical experiments. Figure 3 shows the same domain for the three finest resolutions that we consider in the numerical experiments.

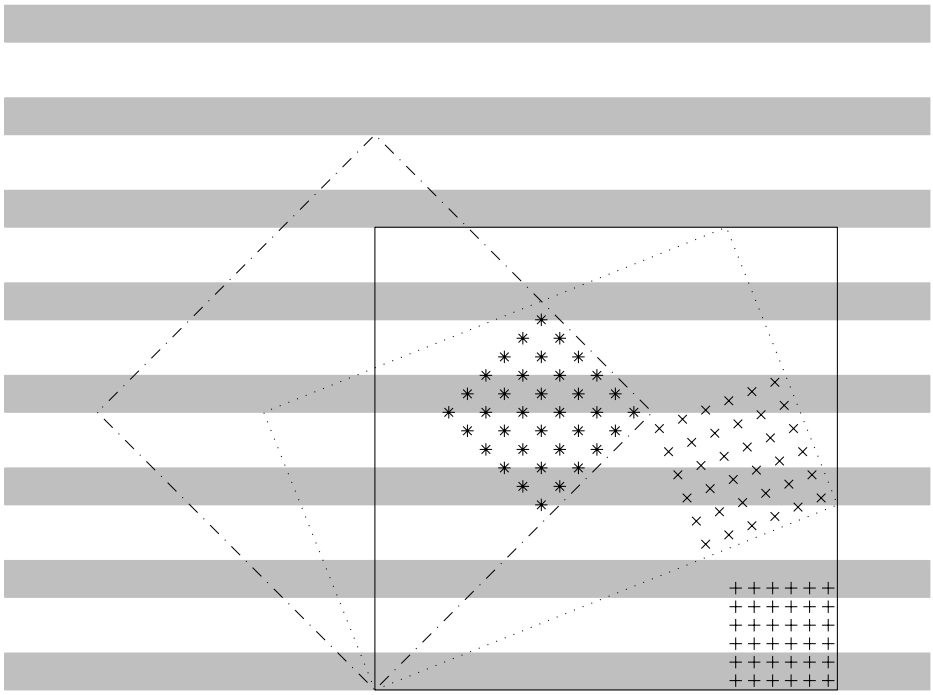

FIGURE 1. *A two-dimensional layered structure with three different representative elementary volumes. They correspond to different choices of coordinate axis with respect to the media. In the "natural" coordinates of the media, corresponding to the solid square, the effective property tensor is diagonal: The entry for the vertical direction equals the harmonic mean of conductivities and the other two diagonal entries are equal to the arithmetic mean. Also illustrated are the coarsest choices of grids used in Table 2 and Table 1.*

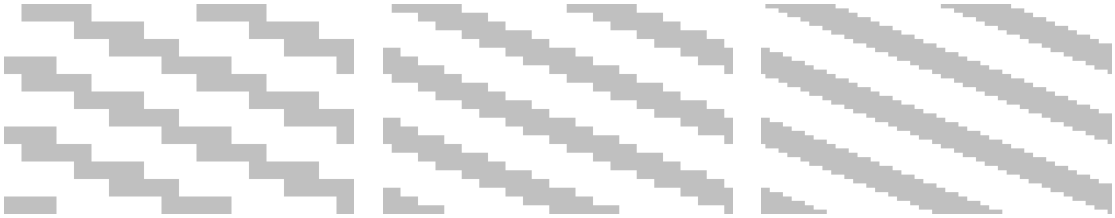

FIGURE 2. $\alpha = \arctan 2/5$ *resolved with a) 20, b) 40 and c) 80 points in the horizontal direction, respectively.*

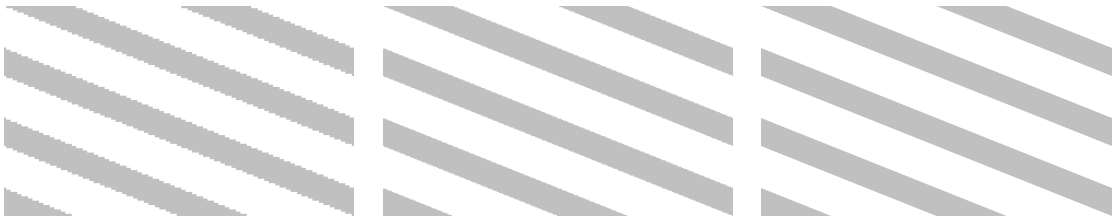

FIGURE 3. $\alpha = \arctan 2/5$ *resolved with a) 160, b) 320 and c) 640 points in the horizontal direction, respectively.*

n_1	n_2	$c=3$	$c=10$	$c=10^2$	$c=10^3$	$c=10^4$	$c=10^8$	Richardson Interpolation
20	12	$4.6\cdot10^{-1}$	$4.3\cdot10^{-1}$	$4.0\cdot10^{-1}$	$4.0\cdot10^{-1}$	$4.0\cdot10^{-1}$	$4.0\cdot10^{-1}$	$4.0\cdot10^{-1}$
40	24	$2.4\cdot10^{-1}$	$2.2\cdot10^{-1}$	$2.1\cdot10^{-1}$	$2.0\cdot10^{-1}$	$2.0\cdot10^{-1}$	$2.0\cdot10^{-1}$	$1.0\cdot10^{-2}$
80	48	$1.2\cdot10^{-1}$	$1.1\cdot10^{-1}$	$1.0\cdot10^{-1}$	$1.0\cdot10^{-1}$	$1.0\cdot10^{-1}$	$1.0\cdot10^{-1}$	$1.2\cdot10^{-3}$
160	96	$5.9\cdot10^{-2}$	$5.5\cdot10^{-2}$	$5.1\cdot10^{-2}$	$5.1\cdot10^{-2}$	$5.0\cdot10^{-2}$	$5.0\cdot10^{-2}$	$7.8\cdot10^{-6}$
320	192	$3.0\cdot10^{-2}$	$2.7\cdot10^{-2}$	$2.5\cdot10^{-2}$	$2.5\cdot10^{-2}$	$2.5\cdot10^{-2}$	$2.5\cdot10^{-2}$	$1.5\cdot10^{-8}$
640	384	$1.5\cdot10^{-2}$	$1.4\cdot10^{-2}$	$1.3\cdot10^{-2}$	$1.3\cdot10^{-2}$	$1.3\cdot10^{-2}$	$1.3\cdot10^{-2}$	$5.6\cdot10^{-11}$

TABLE 1. Relative errors for $\alpha = \arctan 2/5$.

The effective conductivity is given by the generalization of (34) [2],

$$\beta^* = \begin{bmatrix} (\cos\alpha)^2\,\beta^*_{\eta\eta} + (\sin\alpha)^2\,\beta^*_{\xi\xi} & \cos\alpha\sin\alpha\left(\beta^*_{\eta\eta} - \beta^*_{\xi\xi}\right) \\ \cos\alpha\sin\alpha\left(\beta^*_{\eta\eta} - \beta^*_{\xi\xi}\right) & (\sin\alpha)^2\,\beta^*_{\eta\eta} + (\cos\alpha)^2\,\beta^*_{\xi\xi} \end{bmatrix}. \tag{35}$$

Table 1 and Table 2 illustrate the convergence behavior for the two different angles as function of contrast c and resolution, or number of voxels per direction. The entries in the tables are computed as maxima of the relative errors of the 4 components of the effective conductivity tensor. The stopping criterion was a decrease by 8 orders of magnitude of the residual of the Schur-complement. All the calculations in Table 2 took only 2 BiCGStab iterations, and the residual was reduced by 14 orders of magnitude, i.e. 2 iterations solved the linear systems of equations in this case. The calculations in Table 1 took between 4 and 6 iterations. However, the error compared to the analytic values illustrates that it makes no sense to solve the linear system of equations to more than 2 digits of accuracy.

One observes that the relative error is quasi independent of the contrast of the conductivities. The convergence is to first order as the errors half when the number of grid points is doubled. This means that rather fine meshes are needed to achieve reasonable results. For example, 80 grid points in Table 1 yield 11% to 14% relative error, and even 640 grid points yield only 1.3% to 1.5% relative error.

The final column in the tables indicates the relative error that is achieved when Richardson extrapolation [8] is used. Specifically, that column contains the error made for $c = 10^8$ and computing

$$\beta^*_{yy} = \begin{cases} \frac{n_1^{(i)}\beta^{*(i)}_{yy} - n_1^{(i-1)}\beta^{*(i-1)}_{yy}}{n_1^{(i)} - n_1^{(i-1)}} & \text{for } i > 1, \\ \beta^{*(i-1)}_{yy} & \text{for } i = 1. \end{cases}$$

Figure 4 illustrates the behavior of the estimates $\beta^{*(i)}_{yy}$ and the Richardson extrapolant for $c = 1e8$ and $\alpha = \arctan 2/5$ graphically. Richardson extrapolation is known to improve the convergence order of numerical methods, and this can be clearly observed also here. Also noteworthy is that the absolute value of the effective conductivities is systematically underestimated. This is true for all considered layered media examples and seems to indicate that the discretization on voxels overemphasizes the "harmonic mode" of heat conduction.

The Richardson estimate on the second coarsest grid already gives the same quality of the estimate of the effective thermal conductivity as the direct method for the finest grid. The Richardson estimate also shows that the error in the first columns of Table 2 is very regular, probably due to the symmetry of the geometry. This high quality can be taken advantage of in two ways:

- For generated structures, two different grids with different resolutions of the same structure can be generated, and the solutions can be extrapolated to a second order estimate.
- For real images, higher resolution is usually hard to achieve. But if the image is resolved well enough, it may be possible to coarsen the grid, and benefit from Richardson extrapolation on effective conductivities computed on the original and the coarsened grids.

6.2. **Example: Wood fiber composites tomographic data.** Figure 5 shows the view from the top and Figure 6 shows the view from the side on slices of 4 three-dimensional data sets that are tomographic images of tomographed wood fiber composites. From left to right, the density of the samples increases, and in Figure 6 the densification occurs in the vertical image direction while in Figure 5 the densification occurs perpendicular to the slice. The 3 colors represent different materials. The darkest gray is cell wall material, while the light gray and white represent air, where the colors distinguish fiber interior (gray) and fiber exterior air.

The goal of the computations, which will be reported in more detail elsewhere [18], was to see if tomographic images together with numerical computations can be used to model and predict the development of the flow processes during wood composite production and to design composites for thermal insulation properties.

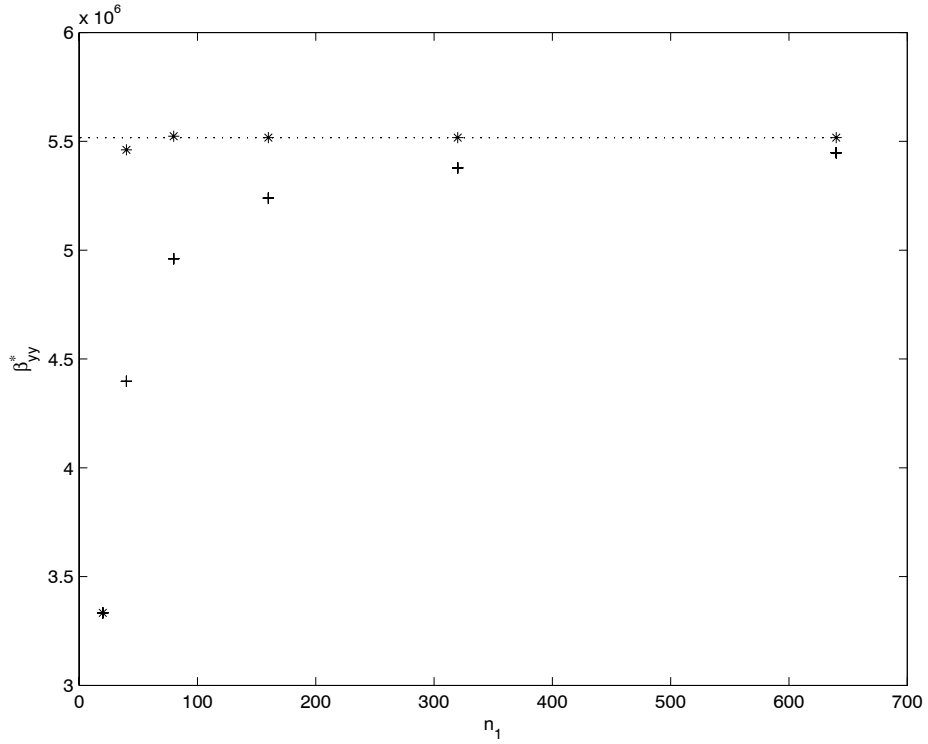

FIGURE 4. *Convergence of the estimated conductivity and impact of Richardson extrapolation. The dotted line shows the analytic value for β^*_{yy} for $c = 10^8$ and $\alpha = \arctan 2/5$. The '+' symbols indicate the results of the first order solver and the '$*$' symbols indicate the estimates based on Richardson extrapolation.*

n_1	n_2	$c = 3$	$c = 10$	$c = 10^2$	$c = 10^3$	$c = 10^4$	$c = 10^8$	Richardson Interpolation
15	15	$4.6 \cdot 10^{-1}$	$4.8 \cdot 10^{-1}$	$5.0 \cdot 10^{-1}$	$5.0 \cdot 10^{-1}$	$5.0 \cdot 10^{-1}$	$5.0 \cdot 10^{-1}$	$5.0 \cdot 10^{-1}$
30	30	$2.3 \cdot 10^{-1}$	$2.4 \cdot 10^{-1}$	$2.5 \cdot 10^{-1}$	$2.5 \cdot 10^{-1}$	$2.5 \cdot 10^{-1}$	$2.5 \cdot 10^{-1}$	$1.7 \cdot 10^{-14}$
60	60	$1.1 \cdot 10^{-1}$	$1.2 \cdot 10^{-1}$	$1.2 \cdot 10^{-1}$	$1.2 \cdot 10^{-1}$	$1.2 \cdot 10^{-1}$	$1.2 \cdot 10^{-1}$	$8.0 \cdot 10^{-14}$
120	120	$5.7 \cdot 10^{-2}$	$6.1 \cdot 10^{-2}$	$6.2 \cdot 10^{-2}$	$6.2 \cdot 10^{-2}$	$6.2 \cdot 10^{-2}$	$6.2 \cdot 10^{-2}$	$3.5 \cdot 10^{-13}$
240	240	$2.9 \cdot 10^{-2}$	$3.0 \cdot 10^{-2}$	$3.1 \cdot 10^{-2}$	$3.1 \cdot 10^{-2}$	$3.1 \cdot 10^{-2}$	$3.1 \cdot 10^{-2}$	$1.3 \cdot 10^{-12}$
495	495	$1.4 \cdot 10^{-2}$	$1.5 \cdot 10^{-2}$	$1.5 \cdot 10^{-2}$	$1.5 \cdot 10^{-2}$	$1.5 \cdot 10^{-2}$	$1.5 \cdot 10^{-2}$	$2.3 \cdot 10^{-12}$

TABLE 2. Relative errors for $\alpha = \pi/4$.

The results are very promising. We used standard thermal conductivity values from the literature. $\beta = 0.421W/(mK)$ for the cell walls in the computations perpendicular to the densification and $\beta = 0.654W/(mK)$ in the computations parallel to the compression, to make up for anisotropic heat conduction properties of the cell material that the solver can not otherwise account for. The thermal conductivity for air was assumed at about $20^\circ C$ as $\beta = 0.026W/(mK)$ in both cases. Figure 7 illustrates that the computed values agree very well with standard approximations from the wood sciences literature [10, 14].

The computations for the wood fiber composites took between 6 and 12 minutes and used between 3.7 and 6.4 GB of memory on a 64 bit AMD opteron machine using FFTW on 4 CPUs.

6.3. **Example: Generated Foam data.** The third example concerns generated three-dimensional data sets. It illustrates the performance of the 3d C++ implementation of EJ-HEAT. The focus is on memory usage and run-time as well as on the influence of anisotropy, material fractions and conductivity contrast, to illustrate some of the possibilities of performing parameter studies.

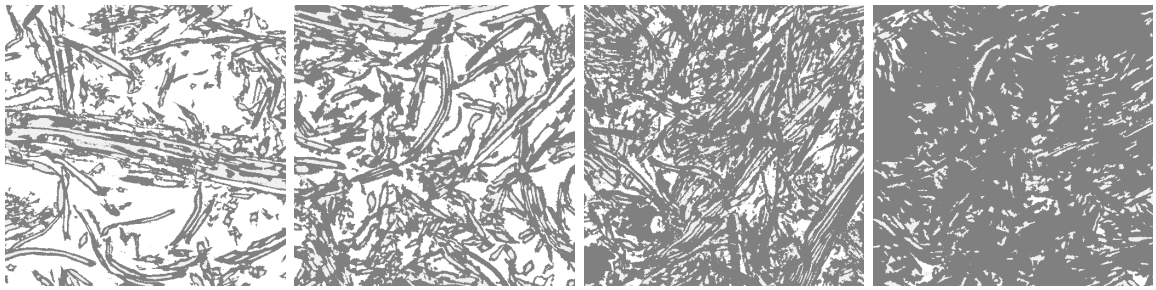

a) b) c) d)

FIGURE 5. *Three-dimensional images of tomographed wood fiber composites. From a) to c), the density of the samples increases,* **the densification occurs perpendicular to the image plane**. *The darkest gray is cell wall material, while the light gray and white represent air.*

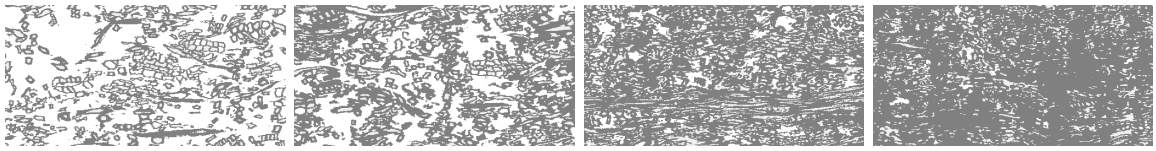

a) b) c) d)

FIGURE 6. *Three-dimensional images of tomographed wood fiber composites. From a) to c), the density of the samples increases,* **the densification occurs in the vertical image direction**. *The darkest gray is cell wall material, while the light gray and white represent air.*

Figure 8 shows x-z cross sections through three-dimensional generated closed pore foams. In this case, the same analytical object is discretized with resolution increasing from left two right. In a), $100 \times 150 \times 200$ grid points are used, in b) $200 \times 300 \times 400$ grid points and in c) $400 \times 600 \times 800$ grid points.

Figure 9 a) shows the same data set as Figure 8 a), but in b) and c) the wall thicknesses are reduced to the minimum possible so that white pores are not connected through a wall either through a voxel face, voxel edge or voxel corner. The figures clearly illustrate the periodicity of the generated foams, at least in the two directions shown.

Table 3 gives the diagonal entries of the effective conductivity tensors, the number of BiCGStab-iterations and run-times to compute these effective conductivities in the case of the materials shown in Figure 8 c) and Figure 9 c). The BiCGStab algorithm was stopped when the norm of the residual of the Schur-complement was reduced by 6 orders of magnitude, and the required memory was 5688 MB for the thin walls and 5500 MB for the thick walls. The contrast is defined as the quotient of the wall conductivity over the pore conductivity. The entries in Table 3 are computed by keeping the pore conductivity fixed at 1 and varying the wall conductivity as 1/1000, 1/10, 1/3, 3, 10 and 1000. The 6 rows of the table correspond to the x-, y- and z- directional thermal conductivities of the thin wall foam in Figure 9 c) and thick wall foam in Figure 8 c).

Table 3 illustrates that the anisotropy of the foams results in different effective conductivities: The pores are shortest in the x-direction and longest in the z-direction. This is directly reflected in the effective thermal conductivity for all contrasts c, the effective conductivity is highest in z- and lowest in x-direction.

Table 3 also shows that the iteration count and consequently, run-times, depend on the contrast: for small contrast, about 20 times fewer iterations are needed than for large contrast.

Even for the rather stringent requirement of reducing the norm by 6 digits, the execution times are quite acceptable between 15 minutes and 3 hours. This is a smaller spread than that of the iteration counts. It shows that for these problem sizes, setup time and I/O time cannot be neglected but add significantly to the users waiting time. Inaccuracy of the run-time measurements accounts also for longer run-times in spite of feterations (row 1, columns 4 and 5 of Table 3).

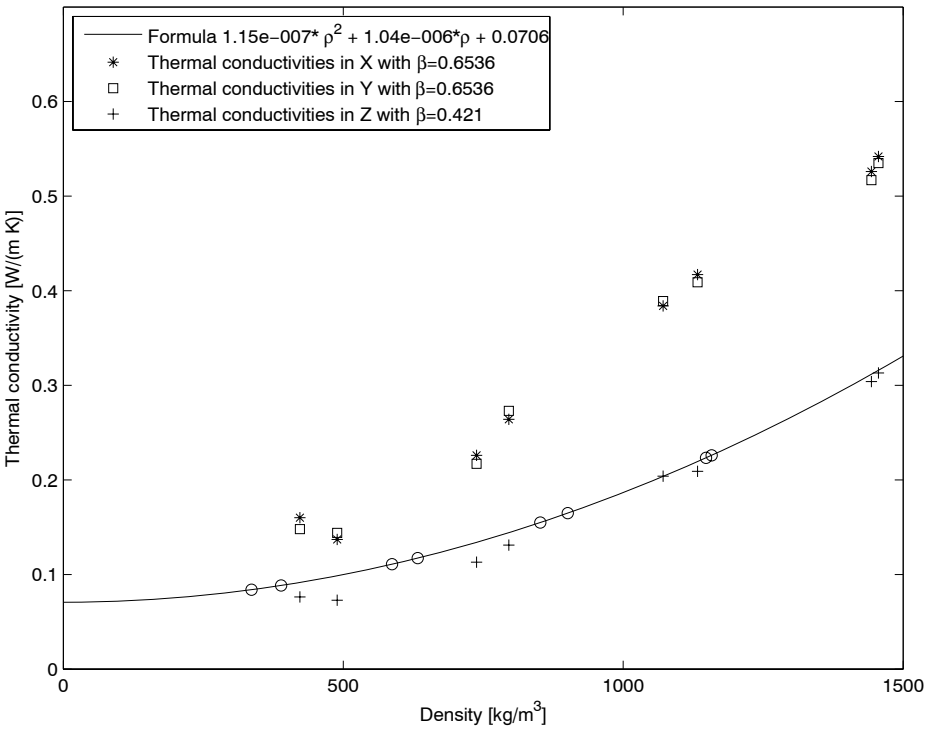

FIGURE 7. *Comparison of literature values for densities of real wood fiber composites (circles,* [14]*) and simulations based on tomographed data sets. The tomographic data contained sligtly more cell material than expected given the specific weight of the cell wall material and the measured density of the real wood fiber composites. So, the simulations results are plotted against densities based on the number of cell wall pixels rather than against the specific weights of the real material. The formula models heat flux through the wood fiber composites and agrees very well with the simulations (crosses). No literature values are available for the in-plane effective conductivity. In these directions the known higher thermal conductivity along the fibers leads to much higher conductivities in the simulations than for the through direction.*

The effective conductivity data data from Table 3 are graphed also in Figure 10. The graph compares as a function of contrast the computed effective conductivities against the well known theoretical bounds, the arithmetic mean and harmonic mean of the conductivities. The computed values lie within the theoretic bounds. For contrast smaller than 1 (walls less conductive than pores) the behavior is more similar to the harmonic mean, while for contrast larger than 1 (walls more conductive than pores), the behavior is more similar to the arithmetic mean.

Table 4 gives more performance data for the computations of effective thermal conductivity. Different from Table 3, also includes computations on the data sets in Figure 9 a) and b) and in Figure 8 a) and b). The iterations, memory usage and time measurements are the maximal values over all contrasts. Usually, this means values for c = 1/000 and computations in the x- or y-directions.

Generally, the thin wall problems are harder to solve than the thick wall problems.

The iteration counts are seen to increase only very moderately under grid refinement, together with Table 3 we conclude that contrast is the main determining factor.

The memory usage increases by much less than the expected factor 8 under grid refinement by a factor 2. This illustrates that the surface data structures (in particular the extra vectors in BiCGStab) require a lot more data per surface point than are required per space point.

Finally, Figure 11 shows that it may not make much sense to solve the Schur-complement problem very accurately. The computed effective conductivities for all 5 different structures in Figure 9 and Figure 8 are plotted against the theoretical bounds. A strong dependence on the relative material fraction is seen. Thus,

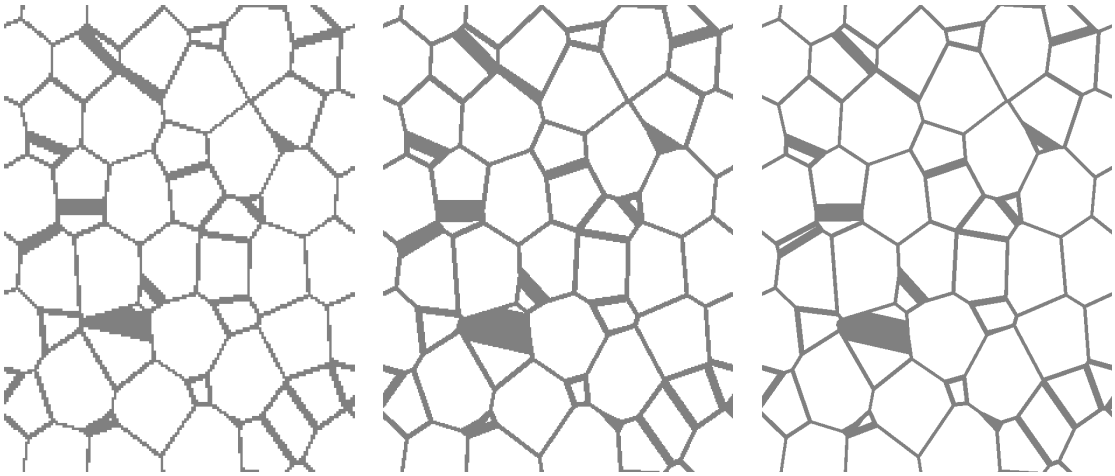

a) b) c)

FIGURE 8. *Grid refinement study of a fixed foam. a)* $100 \times 150 \times 200$ *voxels and 16.3% walls, b)* $200 \times 300 \times 400$ *voxels and 18.8% walls and c)* $400 \times 600 \times 800$ *voxels and 15.0% walls.*

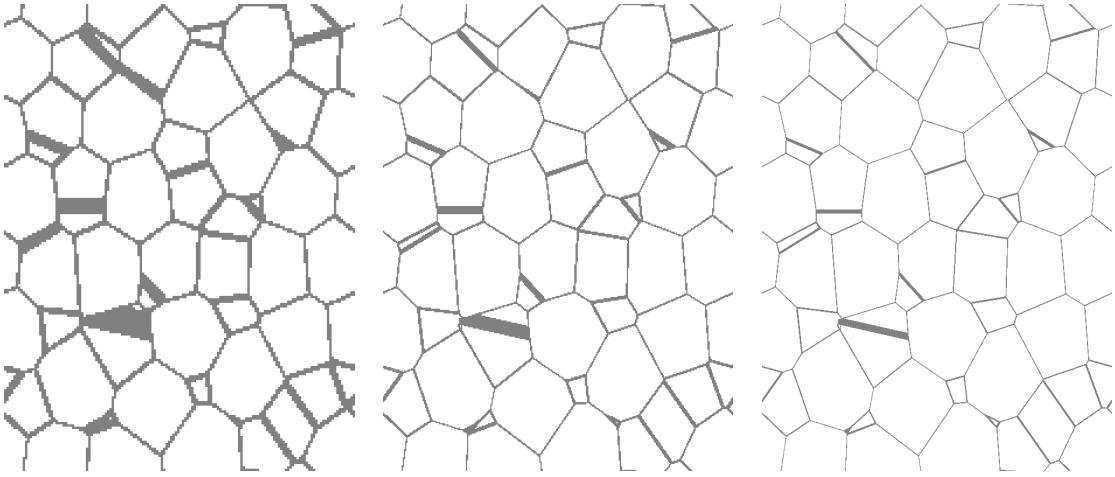

a) b) c)

FIGURE 9. *Material optimization study on the same foam as in Figure 8. a)* $100 \times 150 \times 200$ *voxels and 16.3% walls, b)* $200 \times 300 \times 400$ *voxels and 8.4% walls and c)* $400 \times 600 \times 800$ *voxels and 4.2% walls.*

if the voxelized discretization introduces an error in this material fraction, this error dominates the error in the computed effective conductivity. This error may already occur in the second digit of the conductivity, so that higher accuracy in the solution of the linear system of equations is not required.

Consequently, in applications we usually perform computations with 2 to 3 digits, reducing the norm of the Schur-complement by 2 or 3 orders of magnitude.

The interested reader may download the data sets from the first and third example, the matlab code from Appendix A and C++-based executables from [1] or contact the authors.

7. Conclusions

The homogenization version of a piecewise constant coefficient Poisson problem with complex interface geometry and high contrast is solved using the harmonic averaging discretization. Based on the observation

	x-direction 4.2% walls	y -direction 4.2% walls	z-direction 4.2% walls	x-direction 15.0% walls	y-direction 15.0% walls	z-direction 15.0% walls
c=1/1000,						
β^*_{ii}	5.58e-002	7.72e-002	9.43e-002	1.41e-002	2.00e-002	2.55e-002
Iterations	95	113	100	67	69	59
Time	2:50:44	3:03:24	2:42:22	1:55:32	1:51:05	1:24:24
c= 1/10,						
β^*_{ii}	8.41e-001	8.73e-001	8.89e-001	5.78e-001	6.44e-001	6.82e-001
Iterations	14	15	14	13	12	13
Time	0:28:14	0:28:44	0:27:16	0:26:25	0:27:11	0:25:40
c= 1/3,						
β^*_{ii}	9.47e-001	9.53e-001	9.57e-001	8.30e-001	8.50e-001	8.60e-001
Iterations	7	7	7	6	6	6
Time	0:16:32	0:16:52	0:16:40	0:15:54	0:15:54	0:15:46
c= 3/1,						
β^*_{ii}	1.05e+000	1.06e+000	1.06e+000	1.21e+000	1.24e+000	1.25e+000
Iterations	6	6	6	6	6	6
Time	0:16:05	0:15:55	0:15:43	0:15:45	0:15:44	0:17:08
c= 10/1,						
β^*_{ii}	1.18e+000	1.22e+000	1.24e+000	1.79e+000	1.95e+000	2.03e+000
Iterations	12	11	11	10	11	10
Time	0:24:12	0:23:29	0:23:48	0:22:05	0:23:27	0:21:59
c=1000/1,						
β^*_{ii}	1.70e+001	2.22e+001	2.49e+001	7.97e+001	1.00e+002	1.10e+002
Iterations	36	31	29	17	20	17
Time	1:01:59	0:56:31	0:51:11	0:32:36	0:37:15	0:31:45

TABLE 3. Effective conductivities, iteration counts, and times for the data from Figure 9 c) (left three columns) and Figure 8 c) (right three columns).

n_1	n_2	n_3	variables	iterations	memory (MB)	time h:m:s	walls
100	150	200	3,000,000	69	204	0:01:30	
200	300	400	24,000,000	80	1177	0:12:50	thin
200	300	400	24,000,000	45	1132	0:07:34	thick
400	600	800	192,000,000	113	5688	3:03:24	thin
400	600	800	192,000,000	69	5500	1:55:32	thick

TABLE 4. Iterations, run-time and memory usage for generated foam data.

that away from the interfaces simply the Laplace equation must be solved, the discretization is reformulated in terms of the discontinuities of the normal derivative across the interfaces. This formulation is analogue of finding a single layer charge density in the continuous case and is amenable to using two of the cornerstones of 20th century numerics: a conjugate gradient variant for iteratively solving the Schur-complement, and the Fast Fourier Transformation for inverting the Laplacian in evaluating the Schur-complement matrix.

Very few BiCGStab iterations are needed to solve the Schur-complement which suggests that the formulation yields a rather well-conditioned linear system even in the presence of large contrast in the coefficients. Our treatment of the non-trivial kernel resulting from the periodic boundary conditions and our discretization of the singular right hand side appear to be new in the harmonic averaging context albeit they are standard in the immersed interface context [12].

8. Acknowledgements

The authors thank the members of Fraunhofer ITWM's flow and complex structures department for many helpful discussions on elliptic interface problems. Several industrial projects provided the final need and encouragement to implement the solver.

Vita Rutka, Qing Zhang and Donatas Elvikis, all of ITWM, did much of the work implementing and improving the C++ version of the solver.

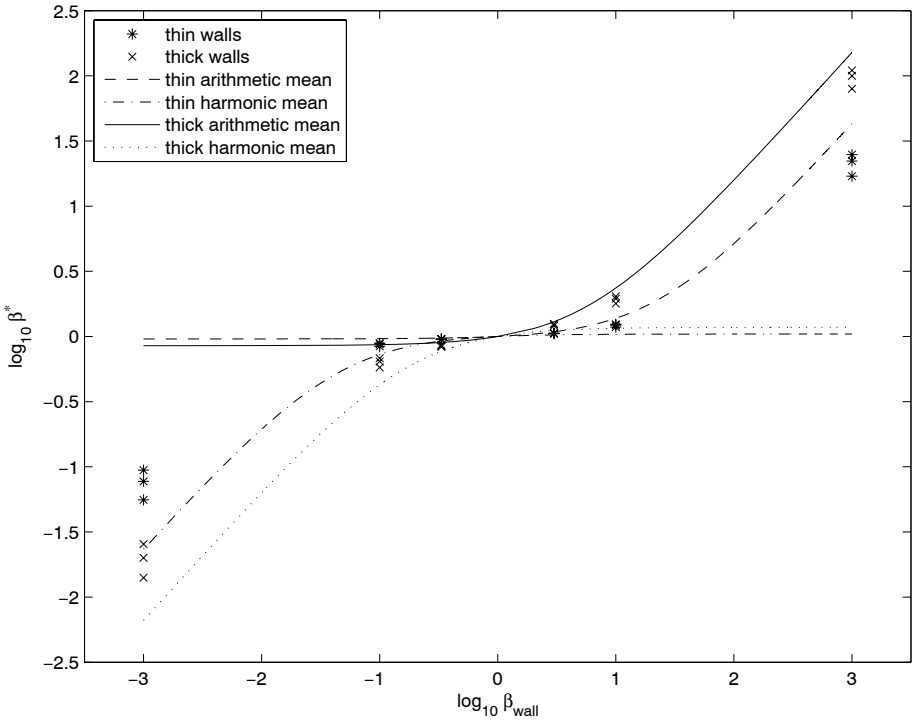

FIGURE 10. *Effective conductivities for the examples in Figure 9 c) and Figure 8 c) as a function of contrast. The behavior changes from "more arithmetic" for contrast smaller than 1 to "more harmonic" for contrast larger than 1.*

Thanks go to Norman Ettrich of ITWM for the generated foam data and to Thomas Walther and Heiko Thömen from the Department of Wood Science at the University of Hamburg and to the Arthur and Aenne Feindt Foundation (Hamburg) for the tomographed pressed wood data.

The computational efficiency of this approach in terms of run times and memory is largely due to the BiCGStab method [9, 21] and FFTW implementation [5].

REFERENCES

[1] http://www.geodict.com/HeatPaper.
[2] A. Bensoussan, J. L. Lions, and G. Papanicolaou. *Asymptotic Analysis for Periodic Structures*. North-Holland, Amsterdam, 1978.
[3] L. J. Durlofsky. A Triangle Based Mixed Finite Element-Finite Volume Technique for Modeling Two Phase Flow through Porous Media. *J. Comput. Phys.*, 105:252–266, April 1993.
[4] R. Fedkiw, T. Aslam, B. Merriman, and S. Osher. A Non-Oscillatory Eulerian Approach to Interfaces in Multimaterial Flows (The Ghost Fluid Method). *J. Comput. Phys.*, 151(2):83–116, 1999.
[5] M. Frigo and S. G. Johnson. The Design and Implementation of FFTW3. *Proceedings of the IEEE*, 93(2):216–231, 2005. Special issue on "Program Generation, Optimization, and Platform Adaptation".
[6] U. Hornung. Introduction. In U. Hornung, editor, *Homogenization and Porous Media*, pages 1—25. Springer, 1997.
[7] S. Hou and X.-D. Liu. A numerical method for solving variable coefficient elliptic equation with interfaces. *J. Comput. Phys.*, 202(2):411–445, 2005.
[8] D. C. Joyce. Survey of Extrapolation Processes in Numerical Analysis. *SIAM Review*, 13(4):435—490, 1971.
[9] C. T. Kelley. *Iterative Methods for Linear and Nonlinear Equations*. Society for Industrial and Applied Mathematics, Philadelphia, 1995.
[10] F. Kollmann and L. Malmquist. Über die Wärmeleitzahl von Holz und Holzwerkstoffen. *Holz als Roh- und Werkstoff*, 14(6):201—204, 1956.
[11] R. J. LeVeque and Z. Li. The Immersed Interface Method for Elliptic Equations with Discontinuous Coefficients and Singular Sources. *SIAM J. Numer. Anal.*, 31:1019—1044, 1994.
[12] R. J. LeVeque and Z. Li. Immersed interface methods for Stokes flow with elastic boundaries or surface tension. *SIAM J. Sci. Comp.*, 18(3):709—735, 1997.
[13] K. Lipnikov, M. Shashkov, and D. Svyatskiy. The mimetic finite difference discretization of diffusion problem on unstructured polyhedral meshes. *J. Comput. Phys.*, 211(2):473–491, 2006.
[14] T. Maku. Studies on the heat conduction in wood. *Wood Research Bulletin, Kyoto University, Japan*, 13:1—80, 1954.
[15] H. Okabe. *Pore-Scale Modelling of Carbonates*. PhD thesis, University of London, 2004.
[16] A. A. Samarskii. *The theory of difference schemes*. Marcel Dekker, Inc., New York, 2001.

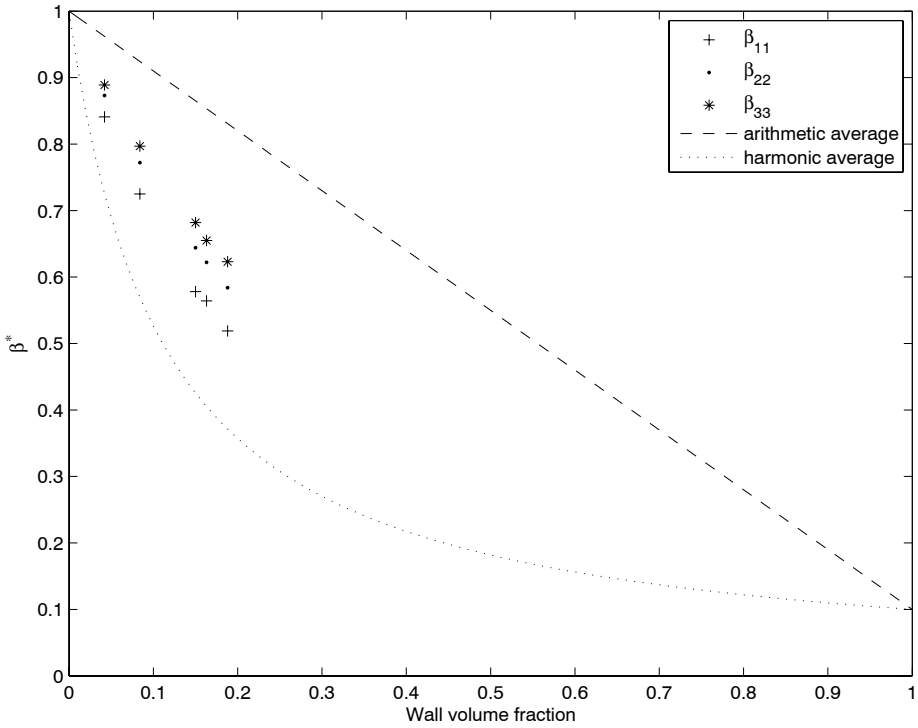

FIGURE 11. *Computed effective conductivities for all 5 different structures in Figure 9 and Figure 8 for $c = 1/10$ and theoretical bounds for $c = 1/10$. A strong dependence of the effective conductivity on material fractions is evident.*

[17] M. Shashkov and S. Steinberg. Solving diffusion equations with rough coefficients in rough grids. *J. Comput. Phys.*, 129(2):383–405, 1996.
[18] H. Thömen, T. Walther, A. Wiegmann, and D. Elvikis. Berechnung der Permeabilität und der Wärmeleitfähigkeit von MDF-Platten anhand von 3D Tomographiedaten. Preprint, 2006.
[19] A. N. Tikhonov and A. A. Samarskii. Homogeneous difference schemes. *USSR Comput. Math. and Math. Phys.*, 1:5—67, 1962.
[20] S. Torquato. *Random Heterogeneous Materials.* Springer: New York, 2002.
[21] H. A. van der Vorst. Bi-CGSTAB: A fast and smoothly converging variant of Bi-CG for the solution of nonsymmetric linear systems. *SIAM J. Sci. Statist. Comput.*, 13:631—644, 1992.
[22] A. Wiegmann. Fast Poisson, fast Helmholtz and fast linear elastostatic solvers on rectangular parallelepipeds. Technical Report LBNL-43565, Lawrence Berkeley National Laboratory, MS 50A-1148, One Cyclotron Rd, Berkeley CA 94720, June 1999.
[23] A. Wiegmann and K. P. Bube. The Explicit–Jump Immersed Interface Method: Finite Difference Methods for PDE with piecewise smooth solutions. *SIAM J. Numer. Anal.*, 37(3):827—862, 2000.

Appendix A. Matlab code for explicit jump effective thermal conductivity

```
function [U,B_1,RR,I] = EJ_heat(S,beta,d,errtol,maxit)
% Explicit jump effective thermal conductivity
% Andreas L. Wiegmann, 25 March 2006.
% S:      3d voxelindices (0-based)
% beta:   conductivities, defined for all indices in S; add 1!
% d:      'x','y' or 'z' direction,
% errtol: desired relative residual for Schur-complement, bicgstab
% maxit:  iteration cap for BiCGStab

global Psi D NX NY NZ H PDM U G B F2 isb isf jsb jsf ksb ksf iind jind kind
[NX,NY,NZ] = size(S);
N          = NX*NY*NZ;
H          = (d=='x')/NX +(d=='y')/NY+(d=='z')/NZ;
B          = zeros(size(S)); % B same size as S also in 1d cases
B(:)       = beta(1+S); % beta indices start with 1, not 0
[i,j,k]    = ind2sub([NX NY NZ],find(B ~= B([end 1:end-1],:,:)));
isb        = mysub2ind(damod(i-1,NX),j,k);
isf        = mysub2ind(      i      ,j,k);
[i,j,k]    = ind2sub([NX NY NZ],find(B ~= B(:,[end 1:end-1],:)));
jsb        = mysub2ind(i,damod(j-1,NY),k);
jsf        = mysub2ind(i,      j      ,k);
[i,j,k]    = ind2sub([NX NY NZ],find(B ~= B(:,:,[end 1:end-1])));
ksb        = mysub2ind(i,j,damod(k-1,NZ));
ksf        = mysub2ind(i,j,      k      );
li         = length(isf);
lj         = length(jsf);
lk         = length(ksf);
l          = li+lj+lk;
iind       =       [1:li];
jind       =    li+[1:lj];
kind       = lj+li+[1:lk];

Bi         = (B(isf)-B(isb))./(B(isf)+B(isb));
Bj         = (B(jsf)-B(jsb))./(B(jsf)+B(jsb));
Bk         = (B(ksf)-B(ksb))./(B(ksf)+B(ksb));
F2         = -2*[double(d=='x')*Bi(:);double(d=='y')*Bj(:);double(d=='z')*Bk(:)];
Psi        = sparse([isb  isf  jsb  jsf  ksb  ksf ],...
                    [iind iind jind jind kind kind],...
                    -0.5/H*ones(1,2*l),N,l);
D          = sparse([iind  iind jind jind kind kind],...
                    [isf   isb  jsf  jsb  ksf  ksb ],...
                   2/H*[Bi   -Bi   Bj   -Bj  Bk  -Bk  ],l,N);
[MM,NM,LM] = ndgrid(2*(cos((2*pi/NX)*[0:NX-1])-1)/H^2,...
                    2*(cos((2*pi/NY)*[0:NY-1])-1)/H^2,...
                    2*(cos((2*pi/NZ)*[0:NZ-1])-1)/H^2);
PDM        = [MM+NM+LM]; clear MM LM NM
PDM(1,1,1) = 1;
[G,e,I]    = bicgstab('AM',F2,errtol,maxit);
U          = poisson(-Psi*G); clear global PDM
[B_1,RR]   = findBAndRelResidual(N,d);
```

```
%%%%%%%%%%%%%%%%%%%%%%%%%%%%%%%%%%%%%%%%%%%%%%%%%%%%%%%%%%%%%%%%%%%%%%%%
function [B_l,RR] = findBAndRelResidual(N,d);
  global NX NY NZ H U G B F2 isf isb jsf jsb ksf ksb iind jind kind Psi D
  i           = 1:N;
  B           = B(:);

  IF          = damod(i+1,NX)+floor((i-1)/NX)*NX;
  IB          = damod(i-1,NX)+floor((i-1)/NX)*NX;
  US          = U(IF)+U(IB); % begin evaluation of Laplacian
  BS1         = B.*( (U(IF)-U(IB))/2/H + (d=='x')); clear IF IB
  if ~isempty(isb) % iind is "right jump" for isb
    BS1(isb)  = BS1(isb) - B(isb').*G(iind)/4; % (23)
    BS1(isf)  = BS1(isf) + B(isf').*G(iind)/4; % (23)
  end
  B_l(1)      = sum(BS1)/N; clear BS1 % (22)

  JF          = damod(i+NX,NX*NY)+floor((i-1)/(NX*NY))*NX*NY;
  JB          = damod(i-NX,NX*NY)+floor((i-1)/(NX*NY))*NX*NY;
  US          = US+U(JF)+U(JB); % continue Laplacian
  BS2         = B.*( (U(JF)-U(JB))/2/H + (d=='y')); clear JF JB
  if ~isempty(jsb) % jind is "back jump" for jsb
    BS2(jsb)  = BS2(jsb) - B(jsb').*G(jind)/4;
    BS2(jsf)  = BS2(jsf) + B(jsf').*G(jind)/4;
  end
  B_l(2)      = sum(BS2)/N; clear BS2

  KF          = damod(i+NX*NY,NX*NY*NZ);
  KB          = damod(i-NX*NY,NX*NY*NZ);
  US          = US+U(KF)+U(KB); % continue Laplacian
  BS3         = B.*( (U(KF)-U(KB))/2/H + (d=='z')); clear KF KB
  if ~isempty(ksb) % kind is "top jump" for ksb,
    BS3(ksb)  = BS3(ksb) - B(ksb').*G(kind)/4;
    BS3(ksf)  = BS3(ksf) + B(ksf').*G(kind)/4;
  end
  B_l(3)      = sum(BS3)/N; clear BS3

  F           = -Psi*F2;
  if norm(F) < eps
      RR = 0;
  else
      RR          = norm(F-(US-6*U)/H^2+Psi*(D*U))/norm(F);
  end

%%%%%%%%%%%%%%%%%%%%%%%%%%%%%%%%%%%%%%%%%%%%%%%%%%%%%%%%%%%%%%%%%%%%%%%%
function l = mysub2ind(i,j,k);                          global NX NY NZ
if ~isempty(i)
  l = [sub2ind([NX,NY,NZ],i,j,k)]';
else
  l = [];
end

%%%%%%%%%%%%%%%%%%%%%%%%%%%%%%%%%%%%%%%%%%%%%%%%%%%%%%%%%%%%%%%%%%%%%%%%
function d = damod(m,n)
  d = m - floor((m-1)./n).*n;
```

```
%%%%%%%%%%%%%%%%%%%%%%%%%%%%%%%%%%%%%%%%%%%%%%%%%%%%%%%%%%%%%%%%%%%%%%%%
function y = poisson(f);                          global NX NY NZ N PDM
  FM = fftn(reshape(f,NX,NY,NZ));
  UM = FM./PDM;
  y  = real(reshape(ifftn(UM),N,1));

%%%%%%%%%%%%%%%%%%%%%%%%%%%%%%%%%%%%%%%%%%%%%%%%%%%%%%%%%%%%%%%%%%%%%%%%
function y = AM(x);                                        global Psi D
  y = x-D*(poisson(Psi*x));

%%%%%%%%%%%%%%%%%%%%%%%%%%%%%%%%%%%%%%%%%%%%%%%%%%%%%%%%%%%%%%%%%%%%%%%%
function [x, error, total_iters] = bicgstab(atv,b, errtol, kmax)
% Bi-CGSTAB solver for linear systems
% C. T. Kelley, December 16, 1994
% adapted by Andreas L. Wiegmann, March 23, 2006
n=length(b);   error=[]; x=zeros(n,1); errtol = errtol*norm(b);
rho   = zeros(kmax+1,1); r     = b; SHOW = false;
hatr0 = r; total_iters = 0; k=0; rho(1)=1; alpha=1; omega=1;
v=zeros(n,1); p=zeros(n,1); rho(2)=hatr0'*r;
zeta=norm(r); error=[error,zeta];
%
while((zeta > errtol) & (k < kmax))
  k = k+1;
  if omega==0
    error('Bi-CGSTAB breakdown, omega=0');
  end
  beta = (rho(k+1)/rho(k))*(alpha/omega);
  p    = r+beta*(p - omega*v);
  v    = feval(atv,p);
  tau  = hatr0'*v;
  if tau==0
    error('Bi-CGSTAB breakdown, tau=0');
  end
  alpha = rho(k+1)/tau;
  s     = r-alpha*v;
  t     = feval(atv,s);
  tau   = t'*t;
  if tau==0
    error('Bi-CGSTAB breakdown, t=0');
  end
  omega       = t'*s/tau;
  rho(k+2)    = -omega*(hatr0'*t);
  x           = x+alpha*p+omega*s;
  r           = s-omega*t;
  zeta        = norm(r);
  total_iters = k;
  error       = [error, zeta];
  if SHOW, disp(['BICGSTAB: ',sprintf('%4d, ',k),...
        'err = ',sprintf('%.16e ',error(k+1)/error(1))]);
  end
end
```

Published reports of the Fraunhofer ITWM

The PDF-files of the following reports are available under:
www.itwm.fraunhofer.de/de/zentral__berichte/berichte

1. D. Hietel, K. Steiner, J. Struckmeier

A Finite - Volume Particle Method for Compressible Flows

We derive a new class of particle methods for conservation laws, which are based on numerical flux functions to model the interactions between moving particles. The derivation is similar to that of classical Finite-Volume methods; except that the fixed grid structure in the Finite-Volume method is substituted by so-called mass packets of particles. We give some numerical results on a shock wave solution for Burgers equation as well as the well-known one-dimensional shock tube problem.
(19 pages, 1998)

2. M. Feldmann, S. Seibold

Damage Diagnosis of Rotors: Application of Hilbert Transform and Multi-Hypothesis Testing

In this paper, a combined approach to damage diagnosis of rotors is proposed. The intention is to employ signal-based as well as model-based procedures for an improved detection of size and location of the damage. In a first step, Hilbert transform signal processing techniques allow for a computation of the signal envelope and the instantaneous frequency, so that various types of non-linearities due to a damage may be identified and classified based on measured response data. In a second step, a multi-hypothesis bank of Kalman Filters is employed for the detection of the size and location of the damage based on the information of the type of damage provided by the results of the Hilbert transform.
Keywords: Hilbert transform, damage diagnosis, Kalman filtering, non-linear dynamics
(23 pages, 1998)

3. Y. Ben-Haim, S. Seibold

Robust Reliability of Diagnostic Multi-Hypothesis Algorithms: Application to Rotating Machinery

Damage diagnosis based on a bank of Kalman filters, each one conditioned on a specific hypothesized system condition, is a well recognized and powerful diagnostic tool. This multi-hypothesis approach can be applied to a wide range of damage conditions. In this paper, we will focus on the diagnosis of cracks in rotating machinery. The question we address is: how to optimize the multi-hypothesis algorithm with respect to the uncertainty of the spatial form and location of cracks and their resulting dynamic effects. First, we formulate a measure of the reliability of the diagnostic algorithm, and then we discuss modifications of the diagnostic algorithm for the maximization of the reliability. The reliability of a diagnostic algorithm is measured by the amount of uncertainty consistent with no-failure of the diagnosis. Uncertainty is quantitatively represented with convex models.
Keywords: Robust reliability, convex models, Kalman filtering, multi-hypothesis diagnosis, rotating machinery, crack diagnosis
(24 pages, 1998)

4. F.-Th. Lentes, N. Siedow

Three-dimensional Radiative Heat Transfer in Glass Cooling Processes

For the numerical simulation of 3D radiative heat transfer in glasses and glass melts, practically applicable mathematical methods are needed to handle such problems optimal using workstation class computers. Since the exact solution would require super-computer capabilities we concentrate on approximate solutions with a high degree of accuracy. The following approaches are studied: 3D diffusion approximations and 3D ray-tracing methods.
(23 pages, 1998)

5. A. Klar, R. Wegener

A hierarchy of models for multilane vehicular traffic
Part I: Modeling

In the present paper multilane models for vehicular traffic are considered. A microscopic multilane model based on reaction thresholds is developed. Based on this model an Enskog like kinetic model is developed. In particular, care is taken to incorporate the correlations between the vehicles. From the kinetic model a fluid dynamic model is derived. The macroscopic coefficients are deduced from the underlying kinetic model. Numerical simulations are presented for all three levels of description in [10]. Moreover, a comparison of the results is given there.
(23 pages, 1998)

Part II: Numerical and stochastic investigations

In this paper the work presented in [6] is continued. The present paper contains detailed numerical investigations of the models developed there. A numerical method to treat the kinetic equations obtained in [6] are presented and results of the simulations are shown. Moreover, the stochastic correlation model used in [6] is described and investigated in more detail.
(17 pages, 1998)

6. A. Klar, N. Siedow

Boundary Layers and Domain Decomposition for Radiative Heat Transfer and Diffusion Equations: Applications to Glass Manufacturing Processes

In this paper domain decomposition methods for radiative transfer problems including conductive heat transfer are treated. The paper focuses on semi-transparent materials, like glass, and the associated conditions at the interface between the materials. Using asymptotic analysis we derive conditions for the coupling of the radiative transfer equations and a diffusion approximation. Several test cases are treated and a problem appearing in glass manufacturing processes is computed. The results clearly show the advantages of a domain decomposition approach. Accuracy equivalent to the solution of the global radiative transfer solution is achieved, whereas computation time is strongly reduced.
(24 pages, 1998)

7. I. Choquet

Heterogeneous catalysis modelling and numerical simulation in rarified gas flows
Part I: Coverage locally at equilibrium

A new approach is proposed to model and simulate numerically heterogeneous catalysis in rarefied gas flows. It is developed to satisfy all together the following points:
1) describe the gas phase at the microscopic scale, as required in rarefied flows,
2) describe the wall at the macroscopic scale, to avoid prohibitive computational costs and consider not only crystalline but also amorphous surfaces,
3) reproduce on average macroscopic laws correlated with experimental results and
4) derive analytic models in a systematic and exact way.
The problem is stated in the general framework of a non static flow in the vicinity of a catalytic and non porous surface (without aging). It is shown that the exact and systematic resolution method based on the Laplace transform, introduced previously by the author to model collisions in the gas phase, can be extended to the present problem. The proposed approach is applied to the modelling of the EleyRideal and LangmuirHinshelwood recombinations, assuming that the coverage is locally at equilibrium. The models are developed considering one atomic species and extended to the general case of several atomic species. Numerical calculations show that the models derived in this way reproduce with accuracy behaviors observed experimentally.
(24 pages, 1998)

8. J. Ohser, B. Steinbach, C. Lang

Efficient Texture Analysis of Binary Images

A new method of determining some characteristics of binary images is proposed based on a special linear filtering. This technique enables the estimation of the area fraction, the specific line length, and the specific integral of curvature. Furthermore, the specific length of the total projection is obtained, which gives detailed information about the texture of the image. The influence of lateral and directional resolution depending on the size of the applied filter mask is discussed in detail. The technique includes a method of increasing directional resolution for texture analysis while keeping lateral resolution as high as possible.
(17 pages, 1998)

9. J. Orlik

Homogenization for viscoelasticity of the integral type with aging and shrinkage

A multiphase composite with periodic distributed inclusions with a smooth boundary is considered in this contribution. The composite component materials are supposed to be linear viscoelastic and aging (of the nonconvolution integral type, for which the Laplace transform with respect to time is not effectively applicable) and are subjected to isotropic shrinkage. The free shrinkage deformation can be considered as a fictitious temperature deformation in the behavior law. The procedure presented in this paper proposes a way to determine average (effective homogenized) viscoelastic and shrinkage (temperature) composite properties and the homogenized stressfield from known properties of the components. This is done by the extension of the asymptotic homogenization technique known for pure elastic nonhomogeneous bodies to the nonhomogeneous thermoviscoelasticity of the integral nonconvolution type. Up to now, the homogenization theory has not covered viscoelasticity of the integral type. SanchezPalencia (1980), Francfort & Suquet (1987) (see [2], [9]) have considered homogenization for viscoelasticity of the differential form and only up to the first derivative order. The integralmodeled viscoelasticity is more general then the differential one and includes almost all known differential models. The homogenization procedure is based on the construction of an asymptotic solution with respect to a period of the composite structure. This reduces the original problem to some auxiliary boundary value problems of elasticity and viscoelasticity on the unit periodic cell, of the same type as the original non-homogeneous problem. The existence and uniqueness results for such problems were obtained for kernels satisfying some constrain conditions. This is done by the extension of the Volterra integral operator theory to the Volterra operators with respect to the time, whose 1 kernels are space linear operators for any fixed time variables. Some ideas of such approach were proposed in [11] and [12], where the Volterra operators with kernels depending additionally on parameter were considered. This manuscript delivers results of the same nature for the case of the spaceoperator kernels.
(20 pages, 1998)

10. J. Mohring

Helmholtz Resonators with Large Aperture

The lowest resonant frequency of a cavity resonator is usually approximated by the classical Helmholtz formula. However, if the opening is rather large and the front wall is narrow this formula is no longer valid. Here we present a correction which is of third order in the ratio of the diameters of aperture and cavity. In addition to the high accuracy it allows to estimate the damping due to radiation. The result is found by applying the method of matched asymptotic expansions. The correction contains form factors describing the shapes of opening and cavity. They are computed for a number of standard geometries. Results are compared with numerical computations.
(21 pages, 1998)

11. H. W. Hamacher, A. Schöbel

On Center Cycles in Grid Graphs

Finding "good" cycles in graphs is a problem of great interest in graph theory as well as in locational analysis. We show that the center and median problems are NP hard in general graphs. This result holds both for the variable cardinality case (i.e. all cycles of the graph are considered) and the fixed cardinality case (i.e. only cycles with a given cardinality p are feasible). Hence it is of interest to investigate special cases where the problem is solvable in polynomial time. In grid graphs, the variable cardinality case is, for instance, trivially solvable if the shape of the cycle can be chosen freely.
If the shape is fixed to be a rectangle one can analyze rectangles in grid graphs with, in sequence, fixed dimension, fixed cardinality, and variable cardinality. In all cases a complete characterization of the optimal cycles and closed form expressions of the optimal objective values are given, yielding polynomial time algorithms for all cases of center rectangle problems.
Finally, it is shown that center cycles can be chosen as rectangles for small cardinalities such that the center cycle problem in grid graphs is in these cases completely solved.
(15 pages, 1998)

12. H. W. Hamacher, K.-H. Küfer

Inverse radiation therapy planning - a multiple objective optimisation approach

For some decades radiation therapy has been proved successful in cancer treatment. It is the major task of clinical radiation treatment planning to realize on the one hand a high level dose of radiation in the cancer tissue in order to obtain maximum tumor control. On the other hand it is obvious that it is absolutely necessary to keep in the tissue outside the tumor, particularly in organs at risk, the unavoidable radiation as low as possible.
No doubt, these two objectives of treatment planning - high level dose in the tumor, low radiation outside the tumor - have a basically contradictory nature. Therefore, it is no surprise that inverse mathematical models with dose distribution bounds tend to be infeasible in most cases. Thus, there is need for approximations compromising between overdosing the organs at risk and underdosing the target volume.
Differing from the currently used time consuming iterative approach, which measures deviation from an ideal (non-achievable) treatment plan using recursively trial-and-error weights for the organs of interest, we go a new way trying to avoid a priori weight choices and consider the treatment planning problem as a multiple objective linear programming problem: with each organ of interest, target tissue as well as organs at risk, we associate an objective function measuring the maximal deviation from the prescribed doses.
We build up a data base of relatively few efficient solutions representing and approximating the variety of Pareto solutions of the multiple objective linear programming problem. This data base can be easily scanned by physicians looking for an adequate treatment plan with the aid of an appropriate online tool.
(14 pages, 1999)

13. C. Lang, J. Ohser, R. Hilfer

On the Analysis of Spatial Binary Images

This paper deals with the characterization of microscopically heterogeneous, but macroscopically homogeneous spatial structures. A new method is presented which is strictly based on integral-geometric formulae such as Crofton's intersection formulae and Hadwiger's recursive definition of the Euler number. The corresponding algorithms have clear advantages over other techniques. As an example of application we consider the analysis of spatial digital images produced by means of Computer Assisted Tomography.
(20 pages, 1999)

14. M. Junk

On the Construction of Discrete Equilibrium Distributions for Kinetic Schemes

A general approach to the construction of discrete equilibrium distributions is presented. Such distribution functions can be used to set up Kinetic Schemes as well as Lattice Boltzmann methods. The general principles are also applied to the construction of Chapman Enskog distributions which are used in Kinetic Schemes for compressible Navier-Stokes equations.
(24 pages, 1999)

15. M. Junk, S. V. Raghurame Rao

A new discrete velocity method for Navier-Stokes equations

The relation between the Lattice Boltzmann Method, which has recently become popular, and the Kinetic Schemes, which are routinely used in Computational Fluid Dynamics, is explored. A new discrete velocity model for the numerical solution of Navier-Stokes equations for incompressible fluid flow is presented by combining both the approaches. The new scheme can be interpreted as a pseudo-compressibility method and, for a particular choice of parameters, this interpretation carries over to the Lattice Boltzmann Method.
(20 pages, 1999)

16. H. Neunzert

Mathematics as a Key to Key Technologies

The main part of this paper will consist of examples, how mathematics really helps to solve industrial problems; these examples are taken from our Institute for Industrial Mathematics, from research in the Technomathematics group at my university, but also from ECMI groups and a company called TecMath, which originated 10 years ago from my university group and has already a very successful history.
(39 pages (4 PDF-Files), 1999)

17. J. Ohser, K. Sandau

Considerations about the Estimation of the Size Distribution in Wicksell's Corpuscle Problem

Wicksell's corpuscle problem deals with the estimation of the size distribution of a population of particles, all having the same shape, using a lower dimensional sampling probe. This problem was originary formulated for particle systems occurring in life sciences but its solution is of actual and increasing interest in materials science. From a mathematical point of view, Wicksell's problem is an inverse problem where the interesting size distribution is the unknown part of a Volterra equation. The problem is often regarded ill-posed, because the structure of the integrand implies unstable numerical solutions. The accuracy of the numerical solutions is considered here using the condition number, which allows to compare different numerical methods with different (equidistant) class sizes and which indicates, as one result, that a finite section thickness of the probe reduces the numerical problems. Furthermore, the relative error of estimation is computed which can be split into two parts. One part consists of the relative discretization error that increases for increasing class size, and the second part is related to the relative statistical error which increases with decreasing class size. For both parts, upper bounds can be given and the sum of them indicates an optimal class width depending on some specific constants.
(18 pages, 1999)

18. E. Carrizosa, H. W. Hamacher, R. Klein, S. Nickel

Solving nonconvex planar location problems by finite dominating sets

It is well-known that some of the classical location problems with polyhedral gauges can be solved in polynomial time by finding a finite dominating set, i. e. a finite set of candidates guaranteed to contain at least one optimal location.
In this paper it is first established that this result holds for a much larger class of problems than currently considered in the literature. The model for which this result can be proven includes, for instance, location problems with attraction and repulsion, and location-allocation problems.
Next, it is shown that the approximation of general gauges by polyhedral ones in the objective function of our general model can be analyzed with regard to the subsequent error in the optimal objective value. For the approximation problem two different approaches are described, the sandwich procedure and the greedy algorithm. Both of these approaches lead - for fixed epsilon - to polynomial approximation algorithms with accuracy epsilon for solving the general model considered in this paper.
Keywords: Continuous Location, Polyhedral Gauges, Finite Dominating Sets, Approximation, Sandwich Algorithm, Greedy Algorithm
(19 pages, 2000)

19. A. Becker

A Review on Image Distortion Measures

Within this paper we review image distortion measures. A distortion measure is a criterion that assigns a "quality number" to an image. We distinguish between mathematical distortion measures and those distortion measures in-cooperating a priori knowledge about the imaging devices (e. g. satellite images), image processing algorithms or the human physiology. We will consider representative examples of different kinds of distortion measures and are going to discuss them.
Keywords: Distortion measure, human visual system
(26 pages, 2000)

20. H. W. Hamacher, M. Labbé, S. Nickel, T. Sonneborn

Polyhedral Properties of the Uncapacitated Multiple Allocation Hub Location Problem

We examine the feasibility polyhedron of the uncapacitated hub location problem (UHL) with multiple allocation, which has applications in the fields of air passenger and cargo transportation, telecommunication and postal delivery services. In particular we determine the dimension and derive some classes of facets of this polyhedron. We develop some general rules about lifting facets from the uncapacitated facility location (UFL) for UHL and projecting facets from UHL to UFL. By applying these rules we get a new class of facets for UHL which dominates the inequalities in the original formulation. Thus we get a new formulation of UHL whose constraints are all facet–defining. We show its superior computational performance by benchmarking it on a well known data set.
Keywords: integer programming, hub location, facility location, valid inequalities, facets, branch and cut
(21 pages, 2000)

21. H. W. Hamacher, A. Schöbel

Design of Zone Tariff Systems in Public Transportation

Given a public transportation system represented by its stops and direct connections between stops, we consider two problems dealing with the prices for the customers: The fare problem in which subsets of stops are already aggregated to zones and "good" tariffs have to be found in the existing zone system. Closed form solutions for the fare problem are presented for three objective functions. In the zone problem the design of the zones is part of the problem. This problem is NP hard and we therefore propose three heuristics which prove to be very successful in the redesign of one of Germany's transportation systems.
(30 pages, 2001)

22. D. Hietel, M. Junk, R. Keck, D. Teleaga

The Finite-Volume-Particle Method for Conservation Laws

In the Finite-Volume-Particle Method (FVPM), the weak formulation of a hyperbolic conservation law is discretized by restricting it to a discrete set of test functions. In contrast to the usual Finite-Volume approach, the test functions are not taken as characteristic functions of the control volumes in a spatial grid, but are chosen from a partition of unity with smooth and overlapping partition functions (the particles), which can even move along pre- scribed velocity fields. The information exchange between particles is based on standard numerical flux functions. Geometrical information, similar to the surface area of the cell faces in the Finite-Volume Method and the corresponding normal directions are given as integral quantities of the partition functions. After a brief derivation of the Finite-Volume-Particle Method, this work focuses on the role of the geometric coefficients in the scheme.
(16 pages, 2001)

23. T. Bender, H. Hennes, J. Kalcsics, M. T. Melo, S. Nickel

Location Software and Interface with GIS and Supply Chain Management

The objective of this paper is to bridge the gap between location theory and practice. To meet this objective focus is given to the development of software capable of addressing the different needs of a wide group of users. There is a very active community on location theory encompassing many research fields such as operations research, computer science, mathematics, engineering, geography, economics and marketing. As a result, people working on facility location problems have a very diverse background and also different needs regarding the software to solve these problems. For those interested in non-commercial applications (e. g. students and researchers), the library of location algorithms (LoLA can be of considerable assistance. LoLA contains a collection of efficient algorithms for solving planar, network and discrete facility location problems. In this paper, a detailed description of the functionality of LoLA is presented. In the fields of geography and marketing, for instance, solving facility location problems requires using large amounts of demographic data. Hence, members of these groups (e. g. urban planners and sales managers) often work with geographical information too s. To address the specific needs of these users, LoLA was inked to a geographical information system (GIS) and the details of the combined functionality are described in the paper. Finally, there is a wide group of practitioners who need to solve large problems and require special purpose software with a good data interface. Many of such users can be found, for example, in the area of supply chain management (SCM). Logistics activities involved in strategic SCM include, among others, facility location planning. In this paper, the development of a commercial location software tool is also described. The too is embedded in the Advanced Planner and Optimizer SCM software developed by SAP AG, Walldorf, Germany. The paper ends with some conclusions and an outlook to future activities.

Keywords: facility location, software development, geographical information systems, supply chain management

(48 pages, 2001)

24. H. W. Hamacher, S. A. Tjandra

Mathematical Modelling of Evacuation Problems: A State of Art

This paper details models and algorithms which can be applied to evacuation problems. While it concentrates on building evacuation many of the results are applicable also to regional evacuation. All models consider the time as main parameter, where the travel time between components of the building is part of the input and the overall evacuation time is the output. The paper distinguishes between macroscopic and microscopic evacuation models both of which are able to capture the evacuees' movement over time.

Macroscopic models are mainly used to produce good lower bounds for the evacuation time and do not consider any individual behavior during the emergency situation. These bounds can be used to analyze existing buildings or help in the design phase of planning a building. Macroscopic approaches which are based on dynamic network flow models (minimum cost dynamic flow, maximum dynamic flow, universal maximum flow, quickest path and quickest flow) are described. A special feature of the presented approach is the fact, that travel times of evacuees are not restricted to be constant, but may be density dependent. Using multicriteria optimization priority regions and blockage due to fire or smoke may be considered. It is shown how the modelling can be done using time parameter either as discrete or continuous parameter.

Microscopic models are able to model the individual evacuee's characteristics and the interaction among evacuees which influence their movement. Due to the corresponding huge amount of data one uses simulation approaches. Some probabilistic laws for individual evacuee's movement are presented. Moreover ideas to model the evacuee's movement using cellular automata (CA) and resulting software are presented.

In this paper we will focus on macroscopic models and only summarize some of the results of the microscopic approach. While most of the results are applicable to general evacuation situations, we concentrate on building evacuation.

(44 pages, 2001)

25. J. Kuhnert, S. Tiwari

Grid free method for solving the Poisson equation

A Grid free method for solving the Poisson equation is presented. This is an iterative method. The method is based on the weighted least squares approximation in which the Poisson equation is enforced to be satisfied in every iterations. The boundary conditions can also be enforced in the iteration process. This is a local approximation procedure. The Dirichlet, Neumann and mixed boundary value problems on a unit square are presented and the analytical solutions are compared with the exact solutions. Both solutions matched perfectly.

Keywords: Poisson equation, Least squares method, Grid free method

(19 pages, 2001)

26. T. Götz, H. Rave, D. Reinel-Bitzer, K. Steiner, H. Tiemeier

Simulation of the fiber spinning process

To simulate the influence of process parameters to the melt spinning process a fiber model is used and coupled with CFD calculations of the quench air flow. In the fiber model energy, momentum and mass balance are solved for the polymer mass flow. To calculate the quench air the Lattice Boltzmann method is used. Simulations and experiments for different process parameters and hole configurations are compared and show a good agreement.

Keywords: Melt spinning, fiber model, Lattice Boltzmann, CFD

(19 pages, 2001)

27. A. Zemitis

On interaction of a liquid film with an obstacle

In this paper mathematical models for liquid films generated by impinging jets are discussed. Attention is stressed to the interaction of the liquid film with some obstacle. S. G. Taylor [Proc. R. Soc. London Ser. A 253, 313 (1959)] found that the liquid film generated by impinging jets is very sensitive to properties of the wire which was used as an obstacle. The aim of this presentation is to propose a modification of the Taylor's model, which allows to simulate the film shape in cases, when the angle between jets is different from 180°. Numerical results obtained by discussed models give two different shapes of the liquid film similar as in Taylors experiments. These two shapes depend on the regime: either droplets are produced close to the obstacle or not. The difference between two regimes becomes larger if the angle between jets decreases. Existence of such two regimes can be very essential for some applications of impinging jets, if the generated liquid film can have a contact with obstacles.

Keywords: impinging jets, liquid film, models, numerical solution, shape

(22 pages, 2001)

28. I. Ginzburg, K. Steiner

Free surface lattice-Boltzmann method to model the filling of expanding cavities by Bingham Fluids

The filling process of viscoplastic metal alloys and plastics in expanding cavities is modelled using the lattice Boltzmann method in two and three dimensions. These models combine the regularized Bingham model for viscoplastic with a free-interface algorithm. The latter is based on a modified immiscible lattice Boltzmann model in which one species is the fluid and the other one is considered as vacuum. The boundary conditions at the curved liquid-vacuum interface are met without any geometrical front reconstruction from a first-order Chapman-Enskog expansion. The numerical results obtained with these models are found in good agreement with available theoretical and numerical analysis.

Keywords: Generalized LBE, free-surface phenomena, interface boundary conditions, filling processes, Bingham viscoplastic model, regularized models

(22 pages, 2001)

29. H. Neunzert

»Denn nichts ist für den Menschen als Menschen etwas wert, was er nicht mit Leidenschaft tun kann«
Vortrag anlässlich der Verleihung des Akademiepreises des Landes Rheinland-Pfalz am 21.11.2001

Was macht einen guten Hochschullehrer aus? Auf diese Frage gibt es sicher viele verschiedene, fachbezogene Antworten, aber auch ein paar allgemeine Gesichtspunkte: es bedarf der »Leidenschaft« für die Forschung (Max Weber), aus der dann auch die Begeisterung für die Lehre erwächst. Forschung und Lehre gehören zusammen, um die Wissenschaft als lebendiges Tun vermitteln zu können. Der Vortrag gibt Beispiele dafür, wie in angewandter Mathematik Forschungsaufgaben aus praktischen Alltagsproblemstellungen erwachsen, die in die Lehre auf verschiedenen Stufen (Gymnasium bis Graduiertenkolleg) einfließen; er leitet damit auch zu einem aktuellen Forschungsgebiet, der Mehrskalenanalyse mit ihren vielfältigen Anwendungen in Bildverarbeitung, Materialentwicklung und Strömungsmechanik über, was aber nur kurz gestreift wird. Mathematik erscheint hier als eine moderne Schlüsseltechnologie, die aber auch enge Beziehungen zu den Geistes- und Sozialwissenschaften hat.

Keywords: Lehre, Forschung, angewandte Mathematik, Mehrskalenanalyse, Strömungsmechanik

(18 pages, 2001)

30. J. Kuhnert, S. Tiwari

Finite pointset method based on the projection method for simulations of the incompressible Navier-Stokes equations

A Lagrangian particle scheme is applied to the projection method for the incompressible Navier-Stokes equations. The approximation of spatial derivatives is obtained by the weighted least squares method. The pressure Poisson equation is solved by a local iterative procedure with the help of the least squares method. Numerical tests are performed for two dimensional cases. The Couette flow, Poiseuelle flow, decaying shear flow and the driven cavity flow are presented. The numerical solutions are obtained for stationary as well as instationary cases and are compared with the analytical solutions for channel flows. Finally, the driven cavity in a unit square is considered and the stationary solution obtained from this scheme is compared with that from the finite element method.

Keywords: Incompressible Navier-Stokes equations, Meshfree method, Projection method, Particle scheme, Least squares approximation

AMS subject classification: 76D05, 76M28

(25 pages, 2001)

31. R. Korn, M. Krekel

Optimal Portfolios with Fixed Consumption or Income Streams

We consider some portfolio optimisation problems where either the investor has a desire for an a priori specified consumption stream or/and follows a deterministic pay in scheme while also trying to maximize expected utility from final wealth. We derive explicit closed form solutions for continuous and discrete monetary streams. The mathematical method used is classical stochastic control theory.

Keywords: Portfolio optimisation, stochastic control, HJB equation, discretisation of control problems.

(23 pages, 2002)

32. M. Krekel

Optimal portfolios with a loan dependent credit spread

If an investor borrows money he generally has to pay higher interest rates than he would have received, if he had put his funds on a savings account. The classical model of continuous time portfolio optimisation ignores this effect. Since there is obviously a connection between the default probability and the total per-

centage of wealth, which the investor is in debt, we study portfolio optimisation with a control dependent interest rate. Assuming a logarithmic and a power utility function, respectively, we prove explicit formulae of the optimal control.
Keywords: Portfolio optimisation, stochastic control, HJB equation, credit spread, log utility, power utility, non-linear wealth dynamics
(25 pages, 2002)

33. J. Ohser, W. Nagel, K. Schladitz

The Euler number of discretized sets - on the choice of adjacency in homogeneous lattices

Two approaches for determining the Euler-Poincaré characteristic of a set observed on lattice points are considered in the context of image analysis { the integral geometric and the polyhedral approach. Information about the set is assumed to be available on lattice points only. In order to retain properties of the Euler number and to provide a good approximation of the true Euler number of the original set in the Euclidean space, the appropriate choice of adjacency in the lattice for the set and its background is crucial. Adjacencies are defined using tessellations of the whole space into polyhedrons. In R 3 , two new 14 adjacencies are introduced additionally to the well known 6 and 26 adjacencies. For the Euler number of a set and its complement, a consistency relation holds. Each of the pairs of adjacencies (14:1; 14:1), (14:2; 14:2), (6; 26), and (26; 6) is shown to be a pair of complementary adjacencies with respect to this relation. That is, the approximations of the Euler numbers are consistent if the set and its background (complement) are equipped with this pair of adjacencies. Furthermore, sufficient conditions for the correctness of the approximations of the Euler number are given. The analysis of selected microstructures and a simulation study illustrate how the estimated Euler number depends on the chosen adjacency. It also shows that there is not a uniquely best pair of adjacencies with respect to the estimation of the Euler number of a set in Euclidean space.
Keywords: image analysis, Euler number, neighborhod relationships, cuboidal lattice
(32 pages, 2002)

34. I. Ginzburg, K. Steiner

Lattice Boltzmann Model for Free-Surface flow and Its Application to Filling Process in Casting

A generalized lattice Boltzmann model to simulate free-surface is constructed in both two and three dimensions. The proposed model satisfies the interfacial boundary conditions accurately. A distinctive feature of the model is that the collision processes is carried out only on the points occupied partially or fully by the fluid. To maintain a sharp interfacial front, the method includes an anti-diffusion algorithm. The unknown distribution functions at the interfacial region are constructed according to the first order Chapman-Enskog analysis. The interfacial boundary conditions are satisfied exactly by the coefficients in the Chapman-Enskog expansion. The distribution functions are naturally expressed in the local interfacial coordinates. The macroscopic quantities at the interface are extracted from the least-square solutions of a locally linearized system obtained from the known distribution functions. The proposed method does not require any geometric front construction and is robust for any interfacial topology. Simulation results of realistic filling process are presented: rectangular cavity in two dimensions and Hammer box, Campbell box, Sheffield box, and Motorblock in three dimensions. To enhance the stability at high Reynolds numbers, various upwind-type schemes are developed. Free-slip and no-slip boundary conditions are also discussed.
Keywords: Lattice Boltzmann models; free-surface phenomena; interface boundary conditions; filling processes; injection molding; volume of fluid method; interface boundary conditions; advection-schemes; upwind-schemes
(54 pages, 2002)

35. M. Günther, A. Klar, T. Materne, R. Wegener

Multivalued fundamental diagrams and stop and go waves for continuum traffic equations

In the present paper a kinetic model for vehicular traffic leading to multivalued fundamental diagrams is developed and investigated in detail. For this model phase transitions can appear depending on the local density and velocity of the flow. A derivation of associated macroscopic traffic equations from the kinetic equation is given. Moreover, numerical experiments show the appearance of stop and go waves for highway traffic with a bottleneck.
Keywords: traffic flow, macroscopic equations, kinetic derivation, multivalued fundamental diagram, stop and go waves, phase transitions
(25 pages, 2002)

36. S. Feldmann, P. Lang, D. Prätzel-Wolters

Parameter influence on the zeros of network determinants

To a network N(q) with determinant D(s;q) depending on a parameter vector q Î Rr via identification of some of its vertices, a network N^ (q) is assigned. The paper deals with procedures to find N^ (q), such that its determinant D^ (s;q) admits a factorization in the determinants of appropriate subnetworks, and with the estimation of the deviation of the zeros of D^ from the zeros of D. To solve the estimation problem state space methods are applied.
Keywords: Networks, Equicofactor matrix polynomials, Realization theory, Matrix perturbation theory
(30 pages, 2002)

37. K. Koch, J. Ohser, K. Schladitz

Spectral theory for random closed sets and estimating the covariance via frequency space

A spectral theory for stationary random closed sets is developed and provided with a sound mathematical basis. Definition and proof of existence of the Bartlett spectrum of a stationary random closed set as well as the proof of a Wiener-Khintchine theorem for the power spectrum are used to two ends: First, well known second order characteristics like the covariance can be estimated faster than usual via frequency space. Second, the Bartlett spectrum and the power spectrum can be used as second order characteristics in frequency space. Examples show, that in some cases information about the random closed set is easier to obtain from these characteristics in frequency space than from their real world counterparts.
Keywords: Random set, Bartlett spectrum, fast Fourier transform, power spectrum
(28 pages, 2002)

38. D. d'Humières, I. Ginzburg

Multi-reflection boundary conditions for lattice Boltzmann models

We present a unified approach of several boundary conditions for lattice Boltzmann models. Its general framework is a generalization of previously introduced schemes such as the bounce-back rule, linear or quadratic interpolations, etc. The objectives are two fold: first to give theoretical tools to study the existing boundary conditions and their corresponding accuracy; secondly to design formally third- order accurate boundary conditions for general flows. Using these boundary conditions, Couette and Poiseuille flows are exact solution of the lattice Boltzmann models for a Reynolds number Re = 0 (Stokes limit).
Numerical comparisons are given for Stokes flows in periodic arrays of spheres and cylinders, linear periodic array of cylinders between moving plates and for Navier-Stokes flows in periodic arrays of cylinders for Re < 200. These results show a significant improvement of the overall accuracy when using the linear interpolations instead of the bounce-back reflection (up to an order of magnitude on the hydrodynamics fields). Further improvement is achieved with the new multi-reflection boundary conditions, reaching a level of accuracy close to the quasi-analytical reference solutions, even for rather modest grid resolutions and few points in the narrowest channels. More important, the pressure and velocity fields in the vicinity of the obstacles are much smoother with multi-reflection than with the other boundary conditions.
Finally the good stability of these schemes is highlighted by some simulations of moving obstacles: a cylinder between flat walls and a sphere in a cylinder.
Keywords: lattice Boltzmann equation, boudary condistions, bounce-back rule, Navier-Stokes equation
(72 pages, 2002)

39. R. Korn

Elementare Finanzmathematik

Im Rahmen dieser Arbeit soll eine elementar gehaltene Einführung in die Aufgabenstellungen und Prinzipien der modernen Finanzmathematik gegeben werden. Insbesondere werden die Grundlagen der Modellierung von Aktienkursen, der Bewertung von Optionen und der Portfolio-Optimierung vorgestellt. Natürlich können die verwendeten Methoden und die entwickelte Theorie nicht in voller Allgemeinheit für den Schulunterricht verwendet werden, doch sollen einzelne Prinzipien so heraus gearbeitet werden, dass sie auch an einfachen Beispielen verstanden werden können.
Keywords: Finanzmathematik, Aktien, Optionen, Portfolio-Optimierung, Börse, Lehrerweiterbildung, Mathematikunterricht
(98 pages, 2002)

40. J. Kallrath, M. C. Müller, S. Nickel

Batch Presorting Problems: Models and Complexity Results

In this paper we consider short term storage systems. We analyze presorting strategies to improve the effiency of these storage systems. The presorting task is called Batch PreSorting Problem (BPSP). The BPSP is a variation of an assigment problem, i. e., it has an assigment problem kernel and some additional constraints. We present different types of these presorting problems, introduce mathematical programming formulations and prove the NP-completeness for one type of the BPSP. Experiments are carried out in order to compare the different model formulations and to investigate the behavior of these models.
Keywords: Complexity theory, Integer programming, Assigment, Logistics
(19 pages, 2002)

41. J. Linn

On the frame-invariant description of the phase space of the Folgar-Tucker equation

The Folgar-Tucker equation is used in flow simulations of fiber suspensions to predict fiber orientation depending on the local flow. In this paper, a complete, frame-invariant description of the phase space of this differential equation is presented for the first time.
Key words: fiber orientation, Folgar-Tucker equation, injection molding
(5 pages, 2003)

42. T. Hanne, S. Nickel

A Multi-Objective Evolutionary Algorithm for Scheduling and Inspection Planning in Software Development Projects

In this article, we consider the problem of planning inspections and other tasks within a software development (SD) project with respect to the objectives quality (no. of defects), project duration, and costs. Based on a discrete-event simulation model of SD processes comprising the phases coding, inspection, test, and rework, we present a simplified formulation of the problem as a multiobjective optimization problem. For solving the problem (i. e. finding an approximation of the efficient set) we develop a multiobjective evolutionary algorithm. Details of the algorithm are discussed as well as results of its application to sample problems.
Key words: multiple objective programming, project management and scheduling, software development, evolutionary algorithms, efficient set
(29 pages, 2003)

43. T. Bortfeld , K.-H. Küfer, M. Monz, A. Scherrer, C. Thieke, H. Trinkaus

Intensity-Modulated Radiotherapy - A Large Scale Multi-Criteria Programming Problem -

Radiation therapy planning is always a tight rope walk between dangerous insufficient dose in the target volume and life threatening overdosing of organs at risk. Finding ideal balances between these inherently contradictory goals challenges dosimetrists and physicians in their daily practice. Today's planning systems are typically based on a single evaluation function that measures the quality of a radiation treatment plan. Unfortunately, such a one dimensional approach cannot satisfactorily map the different backgrounds of physicians and the patient dependent necessities. So, too often a time consuming iteration process between evaluation of dose distribution and redefinition of the evaluation function is needed.

In this paper we propose a generic multi-criteria approach based on Pareto's solution concept. For each entity of interest - target volume or organ at risk a structure dependent evaluation function is defined measuring deviations from ideal doses that are calculated from statistical functions. A reasonable bunch of clinically meaningful Pareto optimal solutions are stored in a data base, which can be interactively searched by physicians. The system guarantees dynamical planning as well as the discussion of tradeoffs between different entities.

Mathematically, we model the upcoming inverse problem as a multi-criteria linear programming problem. Because of the large scale nature of the problem it is not possible to solve the problem in a 3D-setting without adaptive reduction by appropriate approximation schemes.

Our approach is twofold: First, the discretization of the continuous problem is based on an adaptive hierarchical clustering process which is used for a local refinement of constraints during the optimization procedure. Second, the set of Pareto optimal solutions is approximated by an adaptive grid of representatives that are found by a hybrid process of calculating extreme compromises and interpolation methods.

Keywords: multiple criteria optimization, representative systems of Pareto solutions, adaptive triangulation, clustering and disaggregation techniques, visualization of Pareto solutions, medical physics, external beam radiotherapy planning, intensity modulated radiotherapy

(31 pages, 2003)

44. T. Halfmann, T. Wichmann

Overview of Symbolic Methods in Industrial Analog Circuit Design

Industrial analog circuits are usually designed using numerical simulation tools. To obtain a deeper circuit understanding, symbolic analysis techniques can additionally be applied. Approximation methods which reduce the complexity of symbolic expressions are needed in order to handle industrial-sized problems.

This paper will give an overview to the field of symbolic analog circuit analysis. Starting with a motivation, the state-of-the-art simplification algorithms for linear as well as for nonlinear circuits are presented. The basic ideas behind the different techniques are described, whereas the technical details can be found in the cited references. Finally, the application of linear and nonlinear symbolic analysis will be shown on two example circuits.

Keywords: CAD, automated analog circuit design, symbolic analysis, computer algebra, behavioral modeling, system simulation, circuit sizing, macro modeling, differential-algebraic equations, index

(17 pages, 2003)

45. S. E. Mikhailov, J. Orlik

Asymptotic Homogenisation in Strength and Fatigue Durability Analysis of Composites

Asymptotic homogenisation technique and two-scale convergence is used for analysis of macro-strength and fatigue durability of composites with a periodic structure under cyclic loading. The linear damage accumulation rule is employed in the phenomenological micro-durability conditions (for each component of the composite) under varying cyclic loading. Both local and non-local strength and durability conditions are analysed. The strong convergence of the strength and fatigue damage measure as the structure period tends to zero is proved and their limiting values are estimated.

Keywords: multiscale structures, asymptotic homogenization, strength, fatigue, singularity, non-local conditions

(14 pages, 2003)

46. P. Domínguez-Marín, P. Hansen, N. Mladenovi´c , S. Nickel

Heuristic Procedures for Solving the Discrete Ordered Median Problem

We present two heuristic methods for solving the Discrete Ordered Median Problem (DOMP), for which no such approaches have been developed so far. The DOMP generalizes classical discrete facility location problems, such as the p-median, p-center and Uncapacitated Facility Location problems. The first procedure proposed in this paper is based on a genetic algorithm developed by Moreno Vega [MV96] for p-median and p-center problems. Additionally, a second heuristic approach based on the Variable Neighborhood Search metaheuristic (VNS) proposed by Hansen & Mladenovic [HM97] for the p-median problem is described. An extensive numerical study is presented to show the efficiency of both heuristics and compare them.

Keywords: genetic algorithms, variable neighborhood search, discrete facility location

(31 pages, 2003)

47. N. Boland, P. Domínguez-Marín, S. Nickel, J. Puerto

Exact Procedures for Solving the Discrete Ordered Median Problem

The Discrete Ordered Median Problem (DOMP) generalizes classical discrete location problems, such as the N-median, N-center and Uncapacitated Facility Location problems. It was introduced by Nickel [16], who formulated it as both a nonlinear and a linear integer program. We propose an alternative integer linear programming formulation for the DOMP, discuss relationships between both integer linear programming formulations, and show how properties of optimal solutions can be used to strengthen these formulations. Moreover, we present a specific branch and bound procedure to solve the DOMP more efficiently. We test the integer linear programming formulations and this branch and bound method computationally on randomly generated test problems.

Keywords: discrete location, Integer programming

(41 pages, 2003)

48. S. Feldmann, P. Lang

Padé-like reduction of stable discrete linear systems preserving their stability

A new stability preserving model reduction algorithm for discrete linear SISO-systems based on their impulse response is proposed. Similar to the Padé approximation, an equation system for the Markov parameters involving the Hankel matrix is considered, that here however is chosen to be of very high dimension. Although this equation system therefore in general cannot be solved exactly, it is proved that the approximate solution, computed via the Moore-Penrose inverse, gives rise to a stability preserving reduction scheme, a property that cannot be guaranteed for the Padé approach. Furthermore, the proposed algorithm is compared to another stability preserving reduction approach, namely the balanced truncation method, showing comparable performance of the reduced systems. The balanced truncation method however starts from a state space description of the systems and in general is expected to be more computational demanding.

Keywords: Discrete linear systems, model reduction, stability, Hankel matrix, Stein equation

(16 pages, 2003)

49. J. Kallrath, S. Nickel

A Polynomial Case of the Batch Presorting Problem

This paper presents new theoretical results for a special case of the batch presorting problem (BPSP). We will show tht this case can be solved in polynomial time. Offline and online algorithms are presented for solving the BPSP. Competetive analysis is used for comparing the algorithms.

Keywords: batch presorting problem, online optimization, competetive analysis, polynomial algorithms, logistics

(17 pages, 2003)

50. T. Hanne, H. L. Trinkaus

knowCube for MCDM – Visual and Interactive Support for Multicriteria Decision Making

In this paper, we present a novel multicriteria decision support system (MCDSS), called knowCube, consisting of components for knowledge organization, generation, and navigation. Knowledge organization rests upon a database for managing qualitative and quantitative criteria, together with add-on information. Knowledge generation serves filling the database via e. g. identification, optimization, classification or simulation. For "finding needles in haycocks", the knowledge navigation component supports graphical database retrieval and interactive, goal-oriented problem solving. Navigation "helpers" are, for instance, cascading criteria aggregations, modifiable metrics, ergonomic interfaces, and customizable visualizations. Examples from real-life projects, e.g. in industrial engineering and in the life sciences, illustrate the application of our MCDSS.

Key words: Multicriteria decision making, knowledge management, decision support systems, visual interfaces, interactive navigation, real-life applications.

(26 pages, 2003)

51. O. Iliev, V. Laptev

On Numerical Simulation of Flow Through Oil Filters

This paper concerns numerical simulation of flow through oil filters. Oil filters consist of filter housing (filter box), and a porous filtering medium, which completely separates the inlet from the outlet. We discuss mathematical models, describing coupled flows in the pure liquid subregions and in the porous filter media, as well as interface conditions between them. Further, we reformulate the problem in fictitious regions method manner, and discuss peculiarities of the numerical algorithm in solving the coupled system. Next, we show numerical results, validating the model and the algorithm. Finally, we present results from simulation of 3-D oil flow through a real car filter.

Keywords: oil filters, coupled flow in plain and porous media, Navier-Stokes, Brinkman, numerical simulation

(8 pages, 2003)

52. W. Dörfler, O. Iliev, D. Stoyanov, D. Vassileva

On a Multigrid Adaptive Refinement Solver for Saturated Non-Newtonian Flow in Porous Media

A multigrid adaptive refinement algorithm for non-Newtonian flow in porous media is presented. The saturated flow of a non-Newtonian fluid is described by the continuity equation and the generalized Darcy law. The resulting second order nonlinear elliptic equation is discretized by a finite volume method on a cell-centered grid. A nonlinear full-multigrid, full-approximation-storage algorithm is implemented. As a smoother, a single grid solver based on Picard linearization and Gauss-Seidel relaxation is used. Further, a local refinement multigrid algorithm on a composite grid is developed. A residual based error indicator is used in the adaptive refinement criterion. A special implementation approach is used, which allows us to perform unstructured local refinement in conjunction with the finite volume discretization. Several results from numerical experiments are presented in order to examine the performance of the solver.

Keywords: Nonlinear multigrid, adaptive refinement, non-Newtonian flow in porous media

(17 pages, 2003)

53. S. Kruse

On the Pricing of Forward Starting Options under Stochastic Volatility

We consider the problem of pricing European forward starting options in the presence of stochastic volatility. By performing a change of measure using the asset

price at the time of strike determination as a numeraire, we derive a closed-form solution based on Heston's model of stochastic volatility.
Keywords: Option pricing, forward starting options, Heston model, stochastic volatility, cliquet options
(11 pages, 2003)

54. O. Iliev, D. Stoyanov

Multigrid – adaptive local refinement solver for incompressible flows

A non-linear multigrid solver for incompressible Navier-Stokes equations, exploiting finite volume discretization of the equations, is extended by adaptive local refinement. The multigrid is the outer iterative cycle, while the SIMPLE algorithm is used as a smoothing procedure. Error indicators are used to define the refinement subdomain. A special implementation approach is used, which allows to perform unstructured local refinement in conjunction with the finite volume discretization. The multigrid - adaptive local refinement algorithm is tested on 2D Poisson equation and further is applied to a lid-driven flows in a cavity (2D and 3D case), comparing the results with bench-mark data. The software design principles of the solver are also discussed.
Keywords: Navier-Stokes equations, incompressible flow, projection-type splitting, SIMPLE, multigrid methods, adaptive local refinement, lid-driven flow in a cavity
(37 pages, 2003)

55. V. Starikovicius

The multiphase flow and heat transfer in porous media

In first part of this work, summaries of traditional Multiphase Flow Model and more recent Multiphase Mixture Model are presented. Attention is being paid to attempts include various heterogeneous aspects into models. In second part, MMM based differential model for two-phase immiscible flow in porous media is considered. A numerical scheme based on the sequential solution procedure and control volume based finite difference schemes for the pressure and saturation-conservation equations is developed. A computer simulator is built, which exploits object-oriented programming techniques. Numerical result for several test problems are reported.
Keywords: Two-phase flow in porous media, various formulations, global pressure, multiphase mixture model, numerical simulation
(30 pages, 2003)

56. P. Lang, A. Sarishvili, A. Wirsen

Blocked neural networks for knowledge extraction in the software development process

One of the main goals of an organization developing software is to increase the quality of the software while at the same time to decrease the costs and the duration of the development process. To achieve this, various decisions e.ecting this goal before and during the development process have to be made by the managers. One appropriate tool for decision support are simulation models of the software life cycle, which also help to understand the dynamics of the software development process. Building up a simulation model requires a mathematical description of the interactions between di.erent objects involved in the development process. Based on experimental data, techniques from the .eld of knowledge discovery can be used to quantify these interactions and to generate new process knowledge based on the analysis of the determined relationships. In this paper blocked neuronal networks and related relevance measures will be presented as an appropriate tool for quanti.cation and validation of qualitatively known dependencies in the software development process.
Keywords: Blocked Neural Networks, Nonlinear Regression, Knowledge Extraction, Code Inspection
(21 pages, 2003)

57. H. Knaf, P. Lang, S. Zeiser

Diagnosis aiding in Regulation Thermography using Fuzzy Logic

The objective of the present article is to give an overview of an application of Fuzzy Logic in Regulation Thermography, a method of medical diagnosis support. An introduction to this method of the complementary medical science based on temperature measurements – so-called thermograms – is provided. The process of modelling the physician's thermogram evaluation rules using the calculus of Fuzzy Logic is explained.
Keywords: fuzzy logic,knowledge representation, expert system
(22 pages, 2003)

58. M.T. Melo, S. Nickel, F. Saldanha da Gama

Largescale models for dynamic multi-commodity capacitated facility location

In this paper we focus on the strategic design of supply chain networks. We propose a mathematical modeling framework that captures many practical aspects of network design problems simultaneously but which have not received adequate attention in the literature. The aspects considered include: dynamic planning horizon, generic supply chain network structure, external supply of materials, inventory opportunities for goods, distribution of commodities, facility configuration, availability of capital for investments, and storage limitations. Moreover, network configuration decisions concerning the gradual relocation of facilities over the planning horizon are considered. To cope with fluctuating demands, capacity expansion and reduction scenarios are also analyzed as well as modular capacity shifts. The relation of the proposed modeling framework with existing models is discussed. For problems of reasonable size we report on our computational experience with standard mathematical programming software. In particular, useful insights on the impact of various factors on network design decisions are provided.
Keywords: supply chain management, strategic planning, dynamic location, modeling
(40 pages, 2003)

59. J. Orlik

Homogenization for contact problems with periodically rough surfaces

We consider the contact of two elastic bodies with rough surfaces at the interface. The size of the micropeaks and valleys is very small compared with the macrosize of the bodies' domains. This makes the direct application of the FEM for the calculation of the contact problem prohibitively costly. A method is developed that allows deriving a macrocontact condition on the interface. The method involves the twoscale asymptotic homogenization procedure that takes into account the microgeometry of the interface layer and the stiffnesses of materials of both domains. The macrocontact condition can then be used in a FEM model for the contact problem on the macrolevel. The averaged contact stiffness obtained allows the replacement of the interface layer in the macromodel by the macrocontact condition.
Keywords: asymptotic homogenization, contact problems
(28 pages, 2004)

60. A. Scherrer, K.-H. Küfer, M. Monz, F. Alonso, T. Bortfeld

IMRT planning on adaptive volume structures – a significant advance of computational complexity

In intensity-modulated radiotherapy (IMRT) planning the oncologist faces the challenging task of finding a treatment plan that he considers to be an ideal compromise of the inherently contradictive goals of delivering a sufficiently high dose to the target while widely sparing critical structures. The search for this a priori unknown compromise typically requires the computation of several plans, i.e. the solution of several optimization problems. This accumulates to a high computational expense due to the large scale of these problems - a consequence of the discrete problem formulation. This paper presents the adaptive clustering method as a new algorithmic concept to overcome these difficulties. The computations are performed on an individually adapted structure of voxel clusters rather than on the original voxels leading to a decisively reduced computational complexity as numerical examples on real clinical data demonstrate. In contrast to many other similar concepts, the typical trade-off between a reduction in computational complexity and a loss in exactness can be avoided: the adaptive clustering method produces the optimum of the original problem. This flexible method can be applied to both single- and multi-criteria optimization methods based on most of the convex evaluation functions used in practice.
Keywords: Intensity-modulated radiation therapy (IMRT), inverse treatment planning, adaptive volume structures, hierarchical clustering, local refinement, adaptive clustering, convex programming, mesh generation, multi-grid methods
(24 pages, 2004)

61. D. Kehrwald

Parallel lattice Boltzmann simulation of complex flows

After a short introduction to the basic ideas of lattice Boltzmann methods and a brief description of a modern parallel computer, it is shown how lattice Boltzmann schemes are successfully applied for simulating fluid flow in microstructures and calculating material properties of porous media. It is explained how lattice Boltzmann schemes compute the gradient of the velocity field without numerical differentiation. This feature is then utilised for the simulation of pseudo-plastic fluids, and numerical results are presented for a simple benchmark problem as well as for the simulation of liquid composite moulding.
Keywords: Lattice Boltzmann methods, parallel computing, microstructure simulation, virtual material design, pseudo-plastic fluids, liquid composite moulding
(12 pages, 2004)

62. O. Iliev, J. Linn, M. Moog, D. Niedziela, V. Starikovicius

On the Performance of Certain Iterative Solvers for Coupled Systems Arising in Discretization of Non-Newtonian Flow Equations

Iterative solution of large scale systems arising after discretization and linearization of the unsteady non-Newtonian Navier–Stokes equations is studied. cross WLF model is used to account for the non-Newtonian behavior of the fluid. Finite volume method is used to discretize the governing system of PDEs. Viscosity is treated explicitely (e.g., it is taken from the previous time step), while other terms are treated implicitly. Different preconditioners (block–diagonal, block–triangular, relaxed incomplete LU factorization, etc.) are used in conjunction with advanced iterative methods, namely, BiCGStab, CGS, GMRES. The action of the preconditioner in fact requires inverting different blocks. For this purpose, in addition to preconditioned BiCGStab, CGS, GMRES, we use also algebraic multigrid method (AMG). The performance of the iterative solvers is studied with respect to the number of unknowns, characteristic velocity in the basic flow, time step, deviation from Newtonian behavior, etc. Results from numerical experiments are presented and discussed.
Keywords: Performance of iterative solvers, Preconditioners, Non-Newtonian flow
(17 pages, 2004)

63. R. Ciegis, O. Iliev, S. Rief, K. Steiner

On Modelling and Simulation of Different Regimes for Liquid Polymer Moulding

In this paper we consider numerical algorithms for solving a system of nonlinear PDEs arising in modeling of liquid polymer injection. We investigate the particular case when a porous preform is located within the mould, so that the liquid polymer flows through a porous medium during the filling stage. The nonlinearity of the governing system of PDEs is due to the non-Newtonian behavior of the polymer, as well as due to the moving free boundary. The latter is related to the penetration front and a Stefan type problem is formulated to account for it. A finite-volume method is used to approximate the given differential problem. Results of numerical experiments are presented.
We also solve an inverse problem and present algorithms for the determination of the absolute preform permeability coefficient in the case when the velocity of the penetration front is known from measurements. In both cases (direct and inverse problems) we emphasize on the specifics related to the non-Newtonian behavior of the polymer. For completeness, we discuss also the Newtonian case. Results of some experimental

measurements are presented and discussed.
Keywords: Liquid Polymer Moulding, Modelling, Simulation, Infiltration, Front Propagation, non-Newtonian flow in porous media
(43 pages, 2004)

64. T. Hanne, H. Neu

Simulating Human Resources in Software Development Processes

In this paper, we discuss approaches related to the explicit modeling of human beings in software development processes. While in most older simulation models of software development processes, esp. those of the system dynamics type, humans are only represented as a labor pool, more recent models of the discrete-event simulation type require representations of individual humans. In that case, particularities regarding the person become more relevant. These individual effects are either considered as stochastic variations of productivity, or an explanation is sought based on individual characteristics, such as skills for instance. In this paper, we explore such possibilities by recurring to some basic results in psychology, sociology, and labor science. Various specific models for representing human effects in software process simulation are discussed.
Keywords: Human resource modeling, software process, productivity, human factors, learning curve
(14 pages, 2004)

65. O. Iliev, A. Mikelic, P. Popov

Fluid structure interaction problems in deformable porous media: Toward permeability of deformable porous media

In this work the problem of fluid flow in deformable porous media is studied. First, the stationary fluid-structure interaction (FSI) problem is formulated in terms of incompressible Newtonian fluid and a linearized elastic solid. The flow is assumed to be characterized by very low Reynolds number and is described by the Stokes equations. The strains in the solid are small allowing for the solid to be described by the Lame equations, but no restrictions are applied on the magnitude of the displacements leading to strongly coupled, nonlinear fluid-structure problem. The FSI problem is then solved numerically by an iterative procedure which solves sequentially fluid and solid subproblems. Each of the two subproblems is discretized by finite elements and the fluid-structure coupling is reduced to an interface boundary condition. Several numerical examples are presented and the results from the numerical computations are used to perform permeability computations for different geometries.
Keywords: fluid-structure interaction, deformable porous media, upscaling, linear elasticity, stokes, finite elements
(28 pages, 2004)

66. F. Gaspar, O. Iliev, F. Lisbona, A. Naumovich, P. Vabishchevich

On numerical solution of 1-D poroelasticity equations in a multilayered domain

Finite volume discretization of Biot system of poroelasticity in a multilayered domain is presented. Staggered grid is used in order to avoid nonphysical oscillations of the numerical solution, appearing when a collocated grid is used. Various numerical experiments are presented in order to illustrate the accuracy of the finite difference scheme. In the first group of experiments, problems having analytical solutions are solved, and the order of convergence for the velocity, the pressure, the displacements, and the stresses is analyzed. In the second group of experiments numerical solution of real problems is presented.
Keywords: poroelasticity, multilayered material, finite volume discretization, MAC type grid
(41 pages, 2004)

67. J. Ohser, K. Schladitz, K. Koch, M. Nöthe

Diffraction by image processing and its application in materials science

A spectral theory for constituents of macroscopically homogeneous random microstructures modeled as homogeneous random closed sets is developed and provided with a sound mathematical basis, where the spectrum obtained by Fourier methods corresponds to the angular intensity distribution of x-rays scattered by this constituent. It is shown that the fast Fourier transform applied to three-dimensional images of microstructures obtained by micro-tomography is a powerful tool of image processing. The applicability of this technique is is demonstrated in the analysis of images of porous media.
Keywords: porous microstructure, image analysis, random set, fast Fourier transform, power spectrum, Bartlett spectrum
(13 pages, 2004)

68. H. Neunzert

Mathematics as a Technology: Challenges for the next 10 Years

No doubt: Mathematics has become a technology in its own right, maybe even a key technology. Technology may be defined as the application of science to the problems of commerce and industry. And science? Science maybe defined as developing, testing and improving models for the prediction of system behavior; the language used to describe these models is mathematics and mathematics provides methods to evaluate these models. Here we are! Why has mathematics become a technology only recently? Since it got a tool, a tool to evaluate complex, "near to reality" models: Computer! The model may be quite old – Navier-Stokes equations describe flow behavior rather well, but to solve these equations for realistic geometry and higher Reynolds numbers with sufficient precision is even for powerful parallel computing a real challenge. Make the models as simple as possible, as complex as necessary – and then evaluate them with the help of efficient and reliable algorithms: These are genuine mathematical tasks.
Keywords: applied mathematics, technology, modelling, simulation, visualization, optimization, glass processing, spinning processes, fiber-fluid interaction, trubulence effects, topological optimization, multicriteria optimization, Uncertainty and Risk, financial mathematics, Malliavin calculus, Monte-Carlo methods, virtual material design, filtration, bio-informatics, system biology
(29 pages, 2004)

69. R. Ewing, O. Iliev, R. Lazarov, A. Naumovich

On convergence of certain finite difference discretizations for 1D poroelasticity interface problems

Finite difference discretizations of 1D poroelasticity equations with discontinuous coefficients are analyzed. A recently suggested FD discretization of poroelasticity equations with constant coefficients on staggered grid, [5], is used as a basis. A careful treatment of the interfaces leads to harmonic averaging of the discontinuous coefficients. Here, convergence for the pressure and for the displacement is proven in certain norms for the scheme with harmonic averaging (HA). Order of convergence 1.5 is proven for arbitrary located interface, and second order convergence is proven for the case when the interface coincides with a grid node. Furthermore, following the ideas from [3], modified HA discretization are suggested for particular cases. The velocity and the stress are approximated with second order on the interface in this case. It is shown that for wide class of problems, the modified discretization provides better accuracy. Second order convergence for modified scheme is proven for the case when the interface coincides with a displacement grid node. Numerical experiments are presented in order to illustrate our considerations.
Keywords: poroelasticity, multilayered material, finite volume discretizations, MAC type grid, error estimates
(26 pages,2004)

70. W. Dörfler, O. Iliev, D. Stoyanov, D. Vassileva

On Efficient Simulation of Non-Newtonian Flow in Saturated Porous Media with a Multigrid Adaptive Refinement Solver

Flow of non-Newtonian in saturated porous media can be described by the continuity equation and the generalized Darcy law. Efficient solution of the resulting second order nonlinear elliptic equation is discussed here. The equation is discretized by a finite volume method on a cell-centered grid. Local adaptive refinement of the grid is introduced in order to reduce the number of unknowns. A special implementation approach is used, which allows us to perform unstructured local refinement in conjunction with the finite volume discretization. Two residual based error indicators are exploited in the adaptive refinement criterion. Second order accurate discretization on the interfaces between refined and non-refined subdomains, as well as on the boundaries with Dirichlet boundary condition, are presented here, as an essential part of the accurate and efficient algorithm. A nonlinear full approximation storage multigrid algorithm is developed especially for the above described composite (coarse plus locally refined) grid approach. In particular, second order approximation around interfaces is a result of a quadratic approximation of slave nodes in the multigrid - adaptive refinement (MG-AR) algorithm. Results from numerical solution of various academic and practice-induced problems are presented and the performance of the solver is discussed.
Keywords: Nonlinear multigrid, adaptive renement, non-Newtonian in porous media
(25 pages, 2004)

71. J. Kalcsics, S. Nickel, M. Schröder

Towards a Unified Territory Design Approach – Applications, Algorithms and GIS Integration

Territory design may be viewed as the problem of grouping small geographic areas into larger geographic clusters called territories in such a way that the latter are acceptable according to relevant planning criteria. In this paper we review the existing literature for applications of territory design problems and solution approaches for solving these types of problems. After identifying features common to all applications we introduce a basic territory design model and present in detail two approaches for solving this model: a classical location–allocation approach combined with optimal split resolution techniques and a newly developed computational geometry based method. We present computational results indicating the efficiency and suitability of the latter method for solving large–scale practical problems in an interactive environment. Furthermore, we discuss extensions to the basic model and its integration into Geographic Information Systems.
Keywords: territory desgin, political districting, sales territory alignment, optimization algorithms, Geographical Information Systems
(40 pages, 2005)

72. K. Schladitz, S. Peters, D. Reinel-Bitzer, A. Wiegmann, J. Ohser

Design of acoustic trim based on geometric modeling and flow simulation for non-woven

In order to optimize the acoustic properties of a stacked fiber non-woven, the microstructure of the non-woven is modeled by a macroscopically homogeneous random system of straight cylinders (tubes). That is, the fibers are modeled by a spatially stationary random system of lines (Poisson line process), dilated by a sphere. Pressing the non-woven causes anisotropy. In our model, this anisotropy is described by a one parametric distribution of the direction of the fibers. In the present application, the anisotropy parameter has to be estimated from 2d reflected light microscopic images of microsections of the non-woven.
After fitting the model, the flow is computed in digitized realizations of the stochastic geometric model using the lattice Boltzmann method. Based on the flow resistivity, the formulas of Delany and Bazley predict the frequency-dependent acoustic absorption of the non-woven in the impedance tube.
Using the geometric model, the description of a non-woven with improved acoustic absorption properties is obtained in the following way: First, the fiber thicknesses, porosity and anisotropy of the fiber system are modified. Then the flow and acoustics simulations are performed in the new sample. These two steps are repeatedc for various sets of parameters. Finally, the set of parameters for the geometric model leading to the best acoustic absorption is chosen.
Keywords: random system of fibers, Poisson line process, flow resistivity, acoustic absorption, Lattice-Boltzmann method, non-woven
(21 pages, 2005)

73. V. Rutka, A. Wiegmann

Explicit Jump Immersed Interface Method for virtual material design of the effective elastic moduli of composite materials

Virtual material design is the microscopic variation of materials in the computer, followed by the numerical evaluation of the effect of this variation on the material's macroscopic properties. The goal of this procedure is an in some sense improved material. Here, we give examples regarding the dependence of the effective elastic moduli of a composite material on the geometry of the shape of an inclusion. A new approach on how to solve such interface problems avoids mesh generation and gives second order accurate results even in the vicinity of the interface.
The Explicit Jump Immersed Interface Method is a finite difference method for elliptic partial differential equations that works on an equidistant Cartesian grid in spite of non-grid aligned discontinuities in equation parameters and solution. Near discontinuities, the standard finite difference approximations are modified by adding correction terms that involve jumps in the function and its derivatives. This work derives the correction terms for two dimensional linear elasticity with piecewise constant coefficients, i. e. for composite materials. It demonstrates numerically convergence and approximation properties of the method.
Keywords: virtual material design, explicit jump immersed interface method, effective elastic moduli, composite materials
(22 pages, 2005)

74. T. Hanne

Eine Übersicht zum Scheduling von Baustellen

Im diesem Dokument werden Aspekte der formalen zeitlichen Planung bzw. des Scheduling für Bauprojekte anhand ausgewählter Literatur diskutiert. Auf allgemeine Aspekte des Scheduling soll dabei nicht eingegangen werden. Hierzu seien als Standard-Referenzen nur Brucker (2004) und Pinedo (1995) genannt. Zu allgemeinen Fragen des Projekt-Managements sei auf Kerzner (2003) verwiesen.
Im Abschnitt 1 werden einige Anforderungen und Besonderheiten der Planung von Baustellen diskutiert. Diese treten allerdings auch in zahlreichen anderen Bereichen der Produktionsplanung und des Projektmanagements auf. In Abschnitt 2 werden dann Aspekte zur Formalisierung von Scheduling-Problemen in der Bauwirtschaft diskutiert, insbesondere Ziele und zu berücksichtigende Restriktionen. Auf eine mathematische Formalisierung wird dabei allerdings verzichtet. Abschnitt 3 bietet eine Übersicht über Verfahren und grundlegende Techniken für die Berechnung von Schedules. In Abschnitt 4 wird ein Überblick über vorhandene Software, zum einen verbreitete Internationale Software, zum anderen deutschsprachige Branchenlösungen, gegeben. Anschließend werden Schlussfolgerungen gezogen und es erfolgt eine Auflistung der Literaturquellen.
Keywords: Projektplanung, Scheduling, Bauplanung, Bauindustrie
(32 pages, 2005)

75. J. Linn

The Folgar–Tucker Model as a Differential Algebraic System for Fiber Orientation Calculation

The Folgar–Tucker equation (FTE) is the model most frequently used for the prediction of fiber orientation (FO) in simulations of the injection molding process for short–fiber reinforced thermoplasts. In contrast to its widespread use in injection molding simulations, little is known about the mathematical properties of the FTE: an investigation of e. g. its phase space M_{FT} has been presented only recently [12]. The restriction of the dependent variable of the FTE to the set M_{FT} turns the FTE into a differential algebraic system (DAS), a fact which is commonly neglected when devising numerical schemes for the integration of the FTE. In this article we present some recent results on the problem of trace stability as well as some introductory material which complements our recent paper [12].
Keywords: fiber orientation, Folgar–Tucker model, invariants, algebraic constraints, phase space, trace stability
(15 pages, 2005)

76. M. Speckert, K. Dreßler, H. Mauch, A. Lion, G. J. Wierda

Simulation eines neuartigen Prüfsystems für Achserprobungen durch MKS-Modellierung einschließlich Regelung

Testing new suspensions based on real load data is performed on elaborate multi channel test rigs. Usually, wheel forces and moments measured during driving maneuvers are reproduced by the test rig. Because of the complicated interaction between test rig and suspension each new rig configuration has to prove its efficiency with respect to the requirements and the configuration might be subject to optimization.
This paper deals with mathematical and physical modeling of a new concept of a test rig which is based on two hexapods. The model contains the geometric configuration as well as the hydraulics and the controller. It is implemented as an ADAMS/Car template and can be combined with different suspension models to get a complete assembly representing the entire test rig. Using this model, all steps required for a real test run such as controller adaptation, drive file iteration and simulation can be performed. Geometric or hydraulic parameters can be modified easily to improve the setup and adapt the system to the suspension and the given load data.
The model supports and accompanies the introduction of the new rig concept and can be used to prepare real tests on a virtual basis. Using both a front and a rear suspension the approach is described and the potentials coming with the simulation are pointed out.
Keywords: virtual test rig, suspension testing, multibody simulation, modeling hexapod test rig, optimization of test rig configuration
(20 pages, 2005)
In deutscher Sprache; bereits erschienen in: VDI-Berichte Nr. 1900, VDI-Verlag GmbH Düsseldorf (2005), Seiten 227-246

77. K.-H. Küfer, M. Monz, A. Scherrer, P. Süss, F. Alonso, A. S. A. Sultan, Th. Bortfeld, D. Craft, Chr. Thieke

Multicriteria optimization in intensity modulated radiotherapy planning

Inverse treatment planning of intensity modulated radiothrapy is a multicriteria optimization problem: planners have to find optimal compromises between a sufficiently highdose intumor tissuethat garantuee a high tumor control, and, dangerous overdosing of critical structures, in order to avoid high normal tissue complcication problems.
The approach presented in this work demonstrates how to state a flexible generic multicriteria model of the IMRT planning problem and how to produce clinically highly relevant Pareto-solutions. The model is imbedded in a principal concept of Reverse Engineering, a general optimization paradigm for design problems. Relevant parts of the Pareto-set are approximated by using extreme compromises as cornerstone solutions, a concept that is always feasible if box constraints for objective funtions are available. A major practical drawback of generic multicriteria concepts trying to compute or approximate parts of the Pareto-set is the high computational effort. This problem can be overcome by exploitation of an inherent asymmetry of the IMRT planning problem and an adaptive approximation scheme for optimal solutions based on an adaptive clustering preprocessing technique. Finally, a coherent approach for calculating and selecting solutions in a real-timeinteractive decision-making process is presented. The paper is concluded with clinical examples and a discussion of ongoing research topics.
Keywords: multicriteria optimization, extreme solutions, real-time decision making, adaptive approximation schemes, clustering methods, IMRT planning, reverse engineering
(51 pages, 2005)

78. S. Amstutz, H. Andrä

A new algorithm for topology optimization using a level-set method

The levelset method has been recently introduced in the field of shape optimization, enabling a smooth representation of the boundaries on a fixed mesh and therefore leading to fast numerical algorithms. However, most of these algorithms use a HamiltonJacobi equation to connect the evolution of the levelset function with the deformation of the contours, and consequently they cannot create any new holes in the domain (at least in 2D). In this work, we propose an evolution equation for the levelset function based on a generalization of the concept of topological gradient. This results in a new algorithm allowing for all kinds of topology changes.
Keywords: shape optimization, topology optimization, topological sensitivity, level-set
(22 pages, 2005)

79. N. Ettrich

Generation of surface elevation models for urban drainage simulation

Traditional methods fail for the purpose of simulating the complete flow process in urban areas as a consequence of heavy rainfall and as required by the European Standard EN-752 since the bi-directional coupling between sewer and surface is not properly handled. The methodology, developed in the BMBF/EUREKA-project RisUrSim, solves this problem by carrying out the runoff on the basis of shallow water equations solved on high-resolution surface grids. Exchange nodes between the sewer and the surface, like inlets and manholes, are located in the computational grid and water leaving the sewer in case of surcharge is further distributed on the surface.
So far, it has been a problem to get the dense topographical information needed to build models suitable for hydrodynamic runoff calculation in urban areas. Recent airborne data collection methods like laser scanning, however, offer a great chance to economically gather densely sampled input data. This paper studies the potential of such laser-scan data sets for urban water hydrodynamics.
Keywords: Flooding, simulation, urban elevation models, laser scanning
(22 pages, 2005)

80. H. Andrä, J. Linn, I. Matei, I. Shklyar, K. Steiner, E. Teichmann

OPTCAST – Entwicklung adäquater Strukturoptimierungsverfahren für Gießereien Technischer Bericht (KURZFASSUNG)

Im vorliegenden Bericht werden die Erfahrungen und Ergebnisse aus dem Projekt **OptCast** zusammengestellt. Das Ziel dieses Projekts bestand (a) in der Anpassung der Methodik der automatischen Strukturoptimierung für Gussteile und (b) in der Entwicklung und Bereitstellung von gießereispezifischen Optimierungstools für Gießereien und Ingenieurbüros.
Gießtechnische Restriktionen lassen sich nicht auf geometrische Restriktionen reduzieren, sondern sind nur über eine Gießsimulation (Erstarrungssimulation und Eigenspannungsanalyse) adäquat erfassbar, da die lokalen Materialeigenschaften des Gussteils nicht nur von der geometrischen Form des Teils, sondern auch vom verwendeten Material abhängen. Wegen dieser Erkenntnis wurde ein neuartiges iteratives Topologieoptimierungsverfahren unter Verwendung der Level-Set-Technik entwickelt, bei dem keine variable Dichte des Materials eingeführt wird. In jeder Iteration wird ein scharfer Rand des Bauteils berechnet. Somit ist die Gießsimulation in den iterativen Optimierungsprozess integrierbar.
Der Bericht ist wie folgt aufgebaut: In Abschnitt 2 wird der Anforderungskatalog erläutert, der sich aus der Bearbeitung von Benchmark-Problemen in der ersten Projektphase ergab. In Abschnitt 3 werden die Benchmark-Probleme und deren Lösung mit den im Projekt entwickelten Tools beschrieben. Abschnitt 4 enthält die Beschreibung der neu entwickelten Schnittstellen und die mathematische Formulierung des Topologieoptimierungsproblems. Im letzten Abschnitt wird das neue Topologieoptimierungsverfahren, das die Simulation des Gießprozesses einschließt, erläutert.
Keywords: Topologieoptimierung, Level-Set-Methode, Gießprozesssimulation, Gießtechnische Restriktionen, CAE-Kette zur Strukturoptimierung
(77 pages, 2005)

81. N. Marheineke, R. Wegener

Fiber Dynamics in Turbulent Flows
Part I: General Modeling Framework

The paper at hand deals with the modeling of turbulence effects on the dynamics of a long slender elastic fiber. Independent of the choice of the drag model, a general aerodynamic force concept is derived on the basis of the velocity field for the randomly fluctuating component of the flow. Its construction as centered differentiable Gaussian field complies thereby with the requirements of the stochastic k-ε turbulence model and Kolmogorov's universal equilibrium theory on local isotropy.

Keywords: fiber-fluid interaction; Cosserat rod; turbulence modeling; Kolmogorov's energy spectrum; double-velocity correlations; differentiable Gaussian fields

Part II: Specific Taylor Drag

In [12], an aerodynamic force concept for a general air drag model is derived on top of a stochastic k-ε description for a turbulent flow field. The turbulence effects on the dynamics of a long slender elastic fiber are particularly modeled by a correlated random Gaussian force and in its asymptotic limit on a macroscopic fiber scale by Gaussian white noise with flow-dependent amplitude. The paper at hand now presents quantitative similarity estimates and numerical comparisons for the concrete choice of a Taylor drag model in a given application.

Keywords: flexible fibers; k-ε turbulence model; fiber-turbulence interaction scales; air drag; random Gaussian aerodynamic force; white noise; stochastic differential equations; ARMA process

(38 pages, 2005)

82. C. H. Lampert, O. Wirjadi

An Optimal Non-Orthogonal Separation of the Anisotropic Gaussian Convolution Filter

We give ananalytical and geometrical treatment of what it means to separate a Gaussian kernel along arbitrary axes in R^n, and we present a separation scheme that allows to efficiently implement anisotropic Gaussian convolution filters in arbitrary dimension. Based on our previous analysis we show that this scheme is optimal with regard to the number of memory accesses and interpolation operations needed.

Our method relies on non-orthogonal convolution axes and works completely in image space. Thus, it avoids the need for an FFT-subroutine. Depending on the accuracy and speed requirements, different interpolation schemes and methods to implement the one-dimensional Gaussian (FIR, IIR) can be integrated. The algorithm is also feasible for hardware that does not contain a floating-point unit.

Special emphasis is laid on analyzing the performance and accuracy of our method. In particular, we show that without anyspecial optimization of the source code, our method can perform anisotropic Gaussian filtering faster than methods relying on the Fast Fourier Transform.

Keywords: Anisotropic Gaussian filter, linear filtering, orientation space, nD image processing, separable filters

(25 pages, 2005)

83. H. Andrä, D. Stoyanov

Error indicators in the parallel finite element solver for linear elasticity DDFEM

This report discusses two approaches for a posteriori error indication in the linear elasticity solver DDFEM: An indicator based on the Richardson extrapolation and Zienkiewicz-Zhu-type indicator.

The solver handles 3D linear elasticity steady-state problems. It uses own input language to de-scribe the mesh and the boundary conditions. Finite element discretization over tetrahedral meshes with first or second order shape functions (hierarchical basis) has been used to resolve the model. The parallelization of the numerical method is based on the domain decomposition approach. DDFEM is highly portable over a set of parallel computer architectures supporting the MPI-standard.

Keywords: linear elasticity, finite element method, hierarchical shape functions, domain decom-position, parallel implementation, a posteriori error estimates

(21 pages, 2006)

84. M. Schröder, I. Solchenbach

Optimization of Transfer Quality in Regional Public Transit

In this paper we address the improvement of transfer quality in public mass transit networks. Generally there are several transit operators offering service and our work is motivated by the question how their timetables can be altered to yield optimized transfer possibilities in the over-all network. To achieve this, only small changes to the timetables are allowed.

The set-up makes it possible to use a quadratic semi-assignment model to solve the optimization problem. We apply this model, equipped with a new way to assess transfer quality, to the solu-tion of four real-world examples. It turns out that improvements in overall transfer quality can be determined by such optimization-based techniques. Therefore they can serve as a first step to-wards a decision support tool for planners of regional transit networks.

Keywords: public transit, transfer quality, quadratic assignment problem

(16 pages, 2006)

85. A. Naumovich, F. J. Gaspar

On a multigrid solver for the three-dimensional Biot poroelasticity system in multilayered domains

In this paper, we present problem-dependent prolongation and problem-dependent restriction for a multigrid solver for the three-dimensional Biot poroelasticity system, which is solved in a multilayered domain. The system is discretized on a staggered grid using the finite volume method. During the discretization, special care is taken of the discontinuous coefficients. For the efficient multigrid solver, a need in operator-dependent restriction and/or prolongation arises. We derive these operators so that they are consistent with the discretization. They account for the discontinuities of the coefficients, as well as for the coupling of the unknowns within the Biot system. A set of numerical experiments shows necessity of use of the operator-dependent restriction and prolongation in the multigrid solver for the considered class of problems.

Keywords: poroelasticity, interface problem, multigrid, operator-dependent prolongation

(11 pages, 2006)

86. S. Panda, R. Wegener, N. Marheineke

Slender Body Theory for the Dynamics of Curved Viscous Fibers

The paper at hand presents a slender body theory for the dynamics of a curved inertial viscous Newtonian fiber. Neglecting surface tension and temperature dependence, the fiber flow is modeled as a three-dimensional free boundary value problem via instationary incompressible Navier-Stokes equations. From regular asymptotic expansions in powers of the slenderness parameter leading-order balance laws for mass (cross-section) and momentum are derived that combine the unrestricted motion of the fiber center-line with the inner viscous transport. The physically reasonable form of the one-dimensional fiber model results thereby from the introduction of the intrinsic velocity that characterizes the convective terms.

Keywords: curved viscous fibers; fluid dynamics; Navier-Stokes equations; free boundary value problem; asymptotic expansions; slender body theory

(14 pages, 2006)

87. E. Ivanov, H. Andrä, A. Kudryavtsev

Domain Decomposition Approach for Automatic Parallel Generation of Tetrahedral Grids

The desire to simulate more and more geometrical and physical features of technical structures and the availability of parallel computers and parallel numerical solvers which can exploit the power of these machines have lead to a steady increase in the number of grid elements used. Memory requirements and computational time are too large for usual serial PCs. An a priori partitioning algorithm for the parallel generation of 3D nonoverlapping compatible unstructured meshes based on a CAD surface description is presented in this paper. Emphasis is given to practical issues and implementation rather than to theoretical complexity. To achieve robustness of the algorithm with respect to the geometrical shape of the structure authors propose to have several or many but relatively simple algorithmic steps. The geometrical domain decomposition approach has been applied. It allows us to use classic 2D and 3D high-quality Delaunay mesh generators for independent and simultaneous volume meshing. Different aspects of load balancing methods are also explored in the paper. The MPI library and SPMD model are used for parallel grid generator implementation. Several 3D examples are shown.

Key words: Grid Generation, Unstructured Grid, Delaunay Triangulation, Parallel Programming, Domain Decomposition, Load Balancing

(18 pages, 2006)

88. S. Tiwari, S. Antonov, D. Hietel, J. Kuhnert, R. Wegener

A Meshfree Method for Simulations of Interactions between Fluids and Flexible Structures

We present the application of a meshfree method for simulations of interaction between fluids and flexible structures. As a flexible structure we consider a sheet of paper. In a twodimensional framework this sheet can be modeled as curve by the dynamical Kirchhoff-Love theory. The external forces taken into account are gravitation and the pressure difference between upper and lower surface of the sheet. This pressure difference is computed using the Finite Pointset Method (FPM) for the incompressible Navier-Stokes equations. FPM is a meshfree, Lagrangian particle method. The dynamics of the sheet are computed by a finite difference method. We show the suitability of the meshfree method for simulations of fluidstructure interaction in several applications

Key words: Meshfree Method, FPM, Fluid Structure Interaction, Sheet of Paper, Dynamical Coupling

(16 pages, 2006)

89. R. Ciegis , O. Iliev, V. Starikovicius, K. Steiner

Numerical Algorithms for Solving Problems of Multiphase Flows in Porous Media

In this paper we discuss numerical algorithms for solving the system of nonlinear PDEs, arising in modelling of two-phase ows in porous media, as well as the proper object oriented implementation of these algorithms. Global pressure model for isothermal two-phase immiscible flow in porous media is considered in this paper. Finite-volume method is used for the space discretization of the system of PDEs. Different time stepping discretizations and linearization approaches are discussed. The main concepts of the PDE software tool MfsolverC++ are given. Numerical results for one realistic problem are presented.

Keywords: nonlinear algorithms, finite-volume method, software tools, porous media, flows

(16 pages, 2006)

90. D. Niedziela, O. Iliev, A. Latz

On 3D Numerical Simulations of Viscoelastic Fluids

In this work we present and solve a class of non–Newtonian viscoelastic fluid flow problems. Models for non-Newtonian fluids can be classified into three large groups depending on the type of the constitutive relation used: algebraic, differential and integral. The first type of models are most simple one, the last are the most physically adequate ones. Here we consider some models from the first and the third groups, and present robust and efficient algorithms for their solution. We present new mathematical model, which belongs to the class of generalized Newtonian models and is able to account for the anisotropy of the viscosity tensor observed in many real liquids. In particular, we discuss a unified model that captures both shear thinning and extensional thickening for complex flows. The resulting large variations of the viscosity tensor in space and time are leading to a strong numerical coupling of the momentum equations due to the appearance of mixed derivatives in the discretization. To treat this strong coupling appropriately, we present two modifications of classical projection methods (like e.g. SIMPLE). In the first modification all momentum equations are solved coupled (i.e. mixed derivative are discretized implicitly) but still iterations are performed between the momen-

tum equations and the continuity equation. The second one is a fully coupled method, where momentum and continuity equation are solved together using a proper preconditioner. The models involving integral constitutive relation which accounts for the history of deformations, result in a system of integro-differential equations. To solve it, we suggest a proper splitting scheme, which treats the integral and the differential parts consecutively. Integral Oldroyd B and Doi Edwards models are used to simulate flows of dilute and concentrated polymer solutions, respectively.
Keywords: non–Newtonian fluids, anisotropic viscosity, integral constitutive equation
(18 pages, 2006)

91. A. Winterfeld

Application of general semi-infinite Programming to Lapidary Cutting Problems

We consider a volume maximization problemarising in gemstone cutting industry. The problem is formulated as a general semi-infnite program(GSIP)and solved using an interior point method developed by Stein. It is shown, that the convexity assumption needed for the convergence of the algorithm can be satisfied by appropriate model-ling. Clustering techniques are used to reduce the number of container constraints, which is necessary to make the subproblems practically tractable. An iterative process consisting of GSIP optimization and adaptive refinement steps is then employed to obtain an optimal solution which is also feasible for the original problem. Some numeri-cal results based on real world data are also presented.
Keywords: large scale optimization, nonlinear programming, general semi-infinite optimization, design centering, clustering
(26 pages, 2006)

92. J. Orlik, A. Ostrovska

Space-Time Finite Element Approximation and Numerical Solution of Hereditary Linear Viscoelasticity Problems

In this paper we suggest a fast numerical approach to treat problems of the hereditary linear viscoelasticity, which results in the system of elliptic partial differential equations in space variables, who's coefficients are Volterra integral operators of the second kind in time. We propose to approximate the relaxation kernels by the product of purely time- and space-dependent terms, which is achieved by their piecewisepolynomial space-interpolation. A priori error estimate was obtained and it was shown, that such approximation does not decrease the convergence order, when an interpolation polynomial is chosen of the same order as the shape functions for the spatial finite element approximation, while the computational effort is significantly reduced.
Keywords: hereditary viscoelasticity; kern approximation by interpolation; space-time finite element approximation, stability and a priori estimate
(24 pages, 2006)

93. V. Rutka, A. Wiegmann, H. Andrä

EJIIM for Calculation of effective Elastic Moduli in 3D Linear Elasticity

The Explicit Jump Immersed Interface Method solves boundary value problems by embedding arbitrary domains in rectangular parallelepipeds and extending the boundary value problem to such a domain. Now the boundary conditions become jump conditions, and separate equations for the discretized solution of the pde and for the jump conditions are written. In thefirst set of equations, the jumps correct standard difference formulas, in the second set of equations solution values from interior grid points are used to compute quantities on the interface. For constant coefficient pde, the first set can be solved very efficiently by direct Fast Fourier transform inversion, and this is used to efficiently evaluate the smaller Schur-complement matrix-vector multiplication in a conjugate gradient approach to find the jumps. Here this approch is applied to the three-dimensional equations of linear elasticity. The resulting method is second order convergent for the displacements in the maximum norm as the grid is refined. It is applied to calculate the effective elastic moduli of fibrous and porous microstructures in three dimensions using the strain energy equivalence principle. From these effective moduli, best estimates under various symmetry assumptions are calculated.
Keywords: Elliptic PDE, linear elasticity, irregular domain, finite differences, fast solvers, effective elastic moduli
(24 pages, 2006)

94. A. Wiegmann, A. Zemitis

EJ-HEAT: A Fast Explicit Jump Harmonic Averaging Solver for the Effective Heat Conductivity of Composite Materials

The stationary heat equation is solved with periodic boundary conditions in geometrically complex composite materials with high contrast in the thermal conductivities of the individual phases. This is achieved by harmonic averaging and explicitly introducing the jumps across the material interfaces as additional variables. The continuity of the heat flux yields the needed extra equations for these variables. A Schur-complent formulation for the new variables is derived that is solved using the FFT and BiCGStab methods.
The EJ-HEAT solver is given as a 3-page Matlab program in the Appendix. The C++ implementation is used for material design studies. It solves 3-dimensional problems with around 190 Mio variables on a 64-bit AMD Opteron desktop system in less than 6 GB memory and in minutes to hours, depending on the contrast and required accuracy.
The approach may also be used to compute effective electric conductivities because they are governed by the stationary heat equation.
Keywords: Stationary heat equation, effective thermal conductivity, explicit jump, discontinuous coefficients, virtual material design, microstructure simulation, EJ-HEAT
(21 pages, 2006)

Status quo: September 2006